

Texas A&M University  
Mechanical Engineering Department  
Turbomachinery Laboratory

# **DYNAMIC RESPONSE OF A ROTOR-AIR BEARING SYSTEM DUE TO BASE INDUCED PERIODIC MOTIONS**

Research Progress Report to the Turbomachinery Research Consortium

**TRC-B&C-1-09**

by

**Luis San Andrés**  
Mast-Childs Professor  
Principal Investigator

**Yaying Niu**  
Research Assistant

Gas Bearings for Oil-Free Turbomachinery  
**TRC Project TEES# 32513/1519B4**

**Period of Performance: November 1 – May 31, 2009**

**May 2009**

# **DYNAMIC RESPONSE OF A ROTOR-AIR BEARING SYSTEM DUE TO BASE INDUCED PERIODIC MOTIONS**

## **Executive Summary**

Oil-free microturbomachinery (MTM) are inevitably subjected to base or foundation excitations: passenger and commercial transportation vehicles experiencing intermittent excitation from road conditions, and (multiple) periodic load excitations from internal combustion (IC) engines in turbochargers, for example. Too large base excitations can produce severe damage, even failure, due to hard collision or rubbing contact between a rotor and its bearings. Therefore, it is paramount to evaluate the reliability of rotor-air bearing systems to withstanding base load excitations.

In 2008, intermittent shock load excitations, up to 30 g (pk-pk), were introduced to a test rig consisting of a small rotor (0.825 kg) supported on two hybrid flexure pivot tilting pad gas bearings (FPTPBs). The experiments demonstrated the reliability of the hybrid gas bearings to withstanding external transient load excitations. Presently, a shaker delivers periodic load excitations to the base plate supporting the rotor-bearing test rig. The whole system, weighing 48 kg, is supported on two soft coil springs and its lowest natural frequency is just  $\sim 5$  Hz. The rod connecting the shaker to the base plate is not affixed rigidly to the test rig base. The rod merely pushes on the base plate and hence the induced based motions are intermittent with multiple impacts and frequencies. As with most practical conditions, the base motion frequencies (5-12 Hz) are low respective to the operating speed of the rotor-bearing system.

Rotor speed coast down tests evidence the rotor-bearing system natural frequency when the gas bearings are supplied with feed pressures increasing from 2.36 to 5.08 bar (ab). The shaker excitations move the rig base plate, which transmits forces into the rotor-bearing system. The recorded rotor response, relative to the bearing housings, contains the main input frequency (5-12 Hz) and its super harmonics; and because of the intermittency of the base motions, it also excites the rotor-bearing system natural frequency. The motion amplitudes at the natural frequency are smaller than the components synchronous with rotor speed. The excitation of the rotor-bearing system natural frequency does not mean the system exhibits rotordynamic instability.

With base induced motions, the rotor motion amplitude at the system natural frequency increases as the gas bearing feed pressure decreases, as the rotor speed increases, and as the shaker input excitation frequency increases (5-12 Hz). Hence, the test rotor-air bearing system is highly sensitive to base motions, intermittent in character, that excite its natural frequency, in particular when the gas bearings are supplied with a low feed pressure.

Predicted rotor motion responses obtained from XLTRC<sup>2</sup>® and an analytical rigid rotor model, both including the (measured) periodic base motions, show good correlation with the measurements.

The research results demonstrate further the applicability of gas bearings into oil-free high speed MTM.

**Note to reader:** PI edited fully the report (English grammar and semantics and technical content) prior to its release to TRC members.

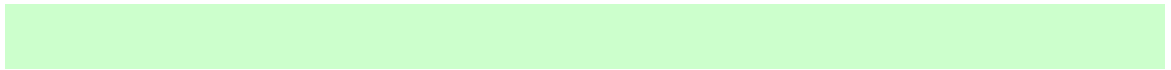


## TABLE OF CONTENTS

	<u>Page</u>
<b>Executive Summary</b>	ii
<b>List of Tables</b>	v
<b>List of Figures</b>	v
<b>Nomenclature</b>	ix
<b>Introduction</b>	1
<b>Literature Review: Rotor-bearing system response due to base or foundation motions</b>	3
<b>Description of Experimental Facility</b>	8
<b>Description of Experimental Procedure</b>	14
<b>Experimental Results</b>	15
<b>Typical base motion induced accelerations</b>	15
<b>Rotor speed coast down tests</b>	17
<b>Rotor motion response at a fixed rotor speed and increasing supply pressures into gas bearings</b>	23
<b>Rotor motion response at a fixed feed pressure into gas bearings and three rotor speeds</b>	27
<b>Rotor motion response for various shaker excitation frequencies</b>	30
<b>Conclusions</b>	34
<b>References</b>	37
<b>Appendix A. Measurement of test rig natural frequency</b>	39
<b>Appendix B. Measurements of rotor coast down speed versus time</b>	42
<b>Appendix C. Predicted stiffness and damping force coefficients for gas bearings</b>	44
<b>Appendix D. XLTRC2® predicted (absolute) rotor motion response due to base excitation</b>	47
<b>Appendix E. Rigid rotor model for prediction of rotor motion response due to base excitation</b>	52

## LIST OF TABLES

		<u>Page</u>
1	Main parameters of test rotor and flexure-pivot tilting-pad bearings	10
2	Sensitivities of sensors	13
D.1	Predicted rotor-bearing system natural frequency at three rotor speeds. Gas bearing supply pressure=2.36 bar (ab).	47
D.2	Measured natural frequency at three rotor speeds. Gas bearing supply pressure=2.36 bar (ab).	48
E.1	Estimated damped natural frequency and mode shapes from rigid rotor model. Gas bearing supply pressure=2.36 bar (ab).	53

## LIST OF FIGURES

		<u>Page</u>
1	Schematic views of hybrid gas bearing test rig modified with shaker to induce base excitations (unit: cm).	9
2	Photograph of test rig with connection to shaker and instrumentation	10
3	Photograph (a) and schematic view (b) of rotor (unit: mm). Location of displacement sensors and bearings noted.	11
4	Photograph and drawings of test hybrid flexure-pivot tilting-pad gas bearing. Noted coordinate system (X: horizontal, Y: vertical) (units: mm)	12
5	Photograph of electromagnetic shaker (LDS V406/8) with power amplifier (PA-100E) and function generator	13
6	Photograph of connection of shaker to test rig base plate	14
7	Typical measured base acceleration in time domain. Shaker excitation frequency: 6 Hz. Rotor speed = 34 krpm (567 Hz)	16
8	Typical measured base acceleration in frequency domain. Shaker excitation frequency: 6 Hz. Rotor speed = 34 krpm (567 Hz)	16
9	Typical measured base acceleration in frequency domain. Shaker excitation frequencies: (a) 5 Hz; (b) 6 Hz; (c) 9 Hz; (d) 12 Hz. Rotor speed = 34 krpm (567 Hz)	17
10	Peak-peak amplitude of rotor synchronous response during rotor speed coast down from 35krpm. Slow roll compensated measurements at rotor left end, vertical direction (LV). No shaker induced excitation. Bearing feed pressures: 2.36, 3.72, and 5.08 bar (ab).	18
11	Peak-peak amplitude of rotor synchronous response during rotor speed coast down from 35krpm. Slow roll compensated measurements at rotor right end, vertical direction (RV). No shaker induced excitation. Bearing feed pressures: 2.36, 3.72, and 5.08 bar (ab).	18
12	Waterfall of rotor motions measured at left end, vertical direction (LV).	20

	No base excitation. Bearing feed pressure: 2.36 bar (ab).	
13	Waterfall of rotor motions measured at left end, vertical direction (LV). Base excitation with main frequency at 12 Hz. Bearing feed pressure: 2.36 bar (ab).	20
14	Waterfall of rotor motions measured at right end, vertical direction (RV). No base excitation. Bearing feed pressure: 2.36 bar (ab).	21
15	Waterfall of rotor motions measured at right end, vertical direction (RV). Base excitation with main frequency at 12 Hz. Bearing feed pressure: 2.36 bar (ab).	21
16	Whirl frequency versus rotor speed for measurements at left end, vertical direction (LV). Shaker induced excitation frequency: 12 Hz. Bearing feed pressure: 2.36 bar (ab).	22
17	Amplitudes of rotor motion versus rotor speed for measurements at left end, vertical direction (LV). Shaker induced excitation frequency: 12 Hz. Bearing feed pressure: 2.36 bar (ab).	22
18	Whirl frequency versus rotor speed for measurements at right end, vertical direction (RV). Shaker induced excitation frequency: 12 Hz. Bearing feed pressure: 2.36 bar (ab).	23
19	Amplitudes of rotor motion versus rotor speed for measurements at right end, vertical direction (RV). Shaker induced excitation frequency: 12 Hz. Bearing feed pressure: 2.36 bar (ab).	23
20	FFT amplitudes of rotor displacement measured at left end, vertical direction (LV). Fixed rotor speed at 34 krpm (567 Hz) and shaker induced excitation frequency at 12 Hz. Bearing feed pressures: 2.36, 3.72, and 5.08 bar (ab).	24
21	FFT amplitudes of rotor displacement measured at right end, vertical direction (RV). Fixed rotor speed at 34 krpm (567 Hz) and shaker induced excitation frequency at 12 Hz. Bearing feed pressures: 2.36, 3.72, and 5.08 bar (ab).	25
22	FFT amplitudes of left bearing force, load cell in vertical direction (FLV). Fixed rotor speed at 34 krpm (567 Hz) and shaker induced excitation frequency at 12 Hz. Bearing feed pressures: 2.36, 3.72, and 5.08 bar (ab).	26
23	FFT amplitudes of right bearing force, load cell in vertical direction (FRV). Fixed rotor speed at 34 krpm (567 Hz) and shaker induced excitation frequency at 12 Hz. Bearing feed pressures: 2.36, 3.72, and 5.08 bar (ab).	26
24	FFT amplitudes of rotor displacement measured at left end, vertical direction (LV). Rotor speed: 26, 30, and 34 krpm. Bearing feed pressure: 2.36 bar (ab). Shaker induced excitation frequency at 12 Hz.	28
25	FFT amplitude of rotor displacement measured at right end, vertical direction (RV). Rotor speed: 26, 30, and 34 krpm. Bearing feed pressure: 2.36 bar (ab). Shaker induced excitation frequency at 12 Hz.	28
26	FFT amplitudes of left bearing force, vertical load cell (FLV). Rotor speed: 26, 30, and 34 krpm. Bearing feed pressure: 2.36 bar (ab). Shaker induced excitation frequency at 12 Hz.	29

27	FFT amplitudes of right bearing force, vertical load cell (FRV). Rotor speed: 26, 30, and 34 krpm. Bearing feed pressure: 2.36 bar (ab). Shaker induced excitation frequency at 12 Hz.	30
28	FFT amplitudes of rotor displacement measured at left end, vertical direction (LV). Shaker induced excitation frequency at 5Hz, 6Hz, 9Hz and 12HZ. Rotor speed: 34 krpm. Bearing feed pressure: 2.36 bar (ab).	31
29	FFT amplitudes of rotor displacement measured at right end, vertical direction (RV). Shaker induced excitation frequency at 5Hz, 6Hz, 9Hz and 12HZ. Rotor speed: 34 krpm. Bearing feed pressure: 2.36 bar (ab).	31
30	FFT amplitudes of left bearing load, from vertical load cell (FLV). Shaker induced excitation frequency at 5Hz, 6Hz, 9Hz and 12HZ. Rotor speed: 34 krpm. Bearing feed pressure: 2.36 bar (ab).	32
31	FFT amplitudes of right bearing load, from vertical load cell (FRV). Shaker induced excitation frequency at 5Hz, 6Hz, 9Hz and 12HZ. Rotor speed: 34 krpm. Bearing feed pressure: 2.36 bar (ab).	33
A.1	Schematic view of test rig and acceleration measurement positions for impact hammer measurements	39
A.2	Accelerations recorded at test rig base plate, motor casing, left bearing housing, and right bearing housing. From impact loads on base plate.	40
A.3	Fig. A.3 Accelerations recorded at motor casing and left end casing. From impact loads on base plate.	40
A.4	Fig. A.4 Accelerations recorded at motor casing and right end casing. From impact loads on base plate.	41
B.1	Measured rotor coast down speed versus time. Shaker induced excitation frequency: 12 Hz. Bearing feed pressures: 2.36, 3.72, and 5.08 bar (ab).	42
B.2	Measured rotor coast down speed versus time. Shaker induced excitation frequencies: 6, 9, and 12 Hz. Bearing feed pressure: 2.36 bar (ab).	43
C.1	Schematic view of the coordinate system. Test rig tilts 10° around the hinged fixture.	44
C.2	Predicted static journal eccentricity ( $e/C$ ) for increasing feed pressures into (left) gas bearing.	45
C.3	Predicted attitude angle for increasing feed pressures into (left) gas bearing.	45
C.4	Stiffness coefficients of gas bearing versus rotor speed. Predictions for increasing supply pressures into bearing. (a) direct and (b) cross-coupled stiffnesses (synchronous speed) coefficients.	45
C.5	Damping coefficients of gas bearing versus rotor speed. Predictions for increasing supply pressures into bearing. (a) direct and (b) cross-coupled damping (synchronous speed) coefficients.	46
D.1	FE structural model of rotor and location of bearing supports	47
D.2	Predicted mode shapes. Forward whirling. Rotor speed: 34 krpm. (a) Conical mode; (b) Cylindrical mode.	48
D.3	Components of base excitation acceleration for prediction of rotor response. Rotor speed: 34 krpm. Main frequency 12 Hz.	49

D.4	Predicted and measured rotor motion amplitude in frequency domain. Left rotor end vertical direction (LV). Input base excitation frequencies for prediction: 12, 24, 36, 48, 60, 185, and 202 Hz. Rotor speed: 26 krpm (433 Hz).	50
D.5	Predicted and measured rotor motion amplitude in frequency domain. Left rotor end vertical direction (LV). Input base excitation frequencies for prediction: 12, 24, 36, 48, 60, 193, and 212 Hz. Rotor speed: 30 krpm (500 Hz).	51
D.6	Predicted and measured rotor motion amplitude in frequency domain. Left rotor end vertical direction (LV). Input base excitation frequencies for prediction: 12, 24, 36, 48, 60, 201, and 222 Hz. Rotor speed: 34 krpm (567 Hz).	51
E.1	Input base excitation acceleration for prediction of rotor response. Rotor speed: 34 krpm. Main excitation frequency 12 Hz.	54
E.2	Predicted and measured rotor response amplitude. Left rotor end vertical direction (LV). Input base excitation frequencies for prediction: 12, 24, 36, 48, 60, 184, and 191 Hz. Rotor speed: 26 krpm (433 Hz).	55
E.3	Predicted and measured rotor response amplitude. Left rotor end vertical direction (LV). Input base excitation frequencies for prediction: 12, 24, 36, 48, 60, 192, and 200 Hz. Rotor speed: 30 krpm (500 Hz).	56
E.4	Predicted and measured rotor response amplitude. Left rotor end vertical direction (LV). Input base excitation frequencies for prediction: 12, 24, 36, 48, 60, 200, and 208 Hz. Rotor speed: 34 krpm (567 Hz).	56
E.5	Comparison of predicted absolute rotor displacements from rigid rotor model and XLTRC <sup>2</sup> ®. Left rotor end vertical direction (LV). Rotor speed: <u>34 krpm</u> (567 Hz).	57



## Nomenclature

<b>A</b>	System parameter matrix, Eq. (E.4)
<b>b</b>	Excitation force vector
<b>C</b>	Viscous damping matrix
$C_b$	Bearing radial clearance [ $\mu\text{m}$ ]
$C_{ij}, i,j = x,y$	Bearing damping coefficient [ $\text{N}\cdot\text{s}/\text{m}$ ]
$d_i, i = 1,2$	Distances from the rotor left and right end planes to the rotor center of gravity [m]
$D_b$	Bearing diameter [mm]
$D_r$	Rotor diameter [mm]
$e$	Journal eccentricity [ $\mu\text{m}$ ]
<b>F<sub>imb</sub></b>	Rotor remnant imbalance force vector
<b>G</b>	Gyroscopic matrix
<b>I</b>	Identity matrix
$I_P$	Rotor polar moments of inertia [ $\text{kg}\cdot\text{m}^2$ ]
$I_T$	Rotor transverse moments of inertia [ $\text{kg}\cdot\text{m}^2$ ]
<b>K</b>	Bearing stiffness matrix
$K_{ij}, i,j = x,y$	Bearing stiffness coefficient [ $\text{MN}/\text{m}$ ]
$l$	Axial distance between two bearing centers [m]
$l_i, i = 1,2$	Distances from the left and right bearing centers to the rotor center of gravity [m]
$L$	Rotor length [mm]
$m$	Rotor mass [kg]
$m_i, i = 1,2$	Rotor remnant imbalance mass on left and right end planes [kg]
<b>M</b>	Inertia matrix
$r_i, i = 1,2$	Radii of the remnant imbalance masses on rotor end planes [m]
$t$	Time [s]
<b>U</b>	Rotor response vector
<b>U<sub>b</sub></b>	Base excitation induced motion vector
<b>W</b>	Rotor static load vector
$W$	Rotor weight [N]
$x_{ij}, i,j = 1,2$	Rotor response along horizontal direction, left and right bearing centers [m]
$X$	Base motion along horizontal direction [m]
$y_{ij}, i,j = 1,2$	Rotor response along vertical direction, left and right bearing centers [m]
$Y$	Base motion along vertical direction [m]
$\Phi_i, i = 1,2$	Angular location (phase) of the remnant imbalance masses [rad]
$\Omega$	Rotor speed [rad/s]
Acronyms	
LV, LH	Left rotor end, vertical and horizontal directions
RV, RH	Right rotor end, vertical and horizontal directions
FLV, FRV	Measured left and right bearing forces from vertically positioned load cells

## Introduction

Gas bearings, offering lesser friction and heat generation than mineral oil lubricated bearings, are used in microturbomachinery (MTM) including turbo expanders, air-cycle turbines for airplanes, and auxiliary power units [1]. Gas bearings do not demand of complex supply and evacuation systems and sealing. Besides, gas film bearings can operate at extremely high and low temperatures.

However, gas bearings have low load carrying capacity and little damping due to the inherently low viscosity of the gas. In addition, hydrodynamic gas bearings with rigid surfaces generate cross-coupled stiffnesses; and thus are prone to self-excited subsynchronous whirl motions leading to rotordynamic instability [2]. Another disadvantage of hydrodynamic gas bearings is their inability to carry load during start-up and shutdown conditions or during abnormal loading events. Lasting solid lubricants (coatings) can aid during these events and avoid excessive friction and premature wear. At times, it is also necessary to supply external pressurized air (as in a hydraulic jack) to enable and maintain early rotor lift-off without damaging contact.

Tilting pad gas bearings permit rotor dynamically stable operation since the bearing pads are free to tilt and do not generate cross-coupled stiffnesses. However, complex mechanical structures and time-consuming installation, along with time-accumulated disadvantages including wear due to high contact stresses at pivot locations, limit their extensive applications in industry [3].

Hybrid flexure-pivot tilting-pad gas bearings (FPTPBs) successfully overcome the drawbacks of conventional tilting-pad gas bearings, since the integral structure of a pad and its supporting thin web pivot contributes to the pads free tilting motion but without contact stress leading to pivot wear. Supplied with a pressurized gas, a rotor supported on FPTPBs achieved a speed of 99 krpm (motor maximum speed) without instability, demonstrating the superior stability of the tested bearings [4].

The current research at TAMU aims to advance the technology of FPTPBs by demonstrating their reliability, durability, and rotordynamic performance. San Andrés [5] advances a model to predict the static load and rotordynamic characteristics of FPTPBs with and without hydrostatic pressurization. In Ref. [4], bearing experimental direct force coefficients correlate well with predictions, thus validating the predictive model. San

Andrés and Ryu [6] perform experiments with severely worn FPTPBs, at load-on-pad (LOP) and load-between-pad (LBP) configurations, and for various imbalance conditions. The test results lend credence to the reliability of the bearings with enlarged and uneven clearances. In addition, automatic regulation of feed pressure in the bearings effectively reduces high motion amplitudes while removing system critical speeds [7].

The ability of withstanding external shocks, random and periodic loads is crucial for gas bearings used in transportation equipment such as turbochargers and micro gas turbine engines. For example, air flow fluctuations and landing sudden maneuver can introduce random excitations or shock to auxiliary power units for aircrafts. Diesel engine induced vibrations and road conditions tend to introduce periodic, or random, or transient excitations to turbochargers. These load excitations could lead to serious failure due to direct impact or rubbing contact between the rotor and bearings. Therefore, it is necessary to evaluate rotor-gas bearing system reliability under operating conditions with external shocks or periodic load excitations introduced into the system.

Ryu and San Andrés [8] perform rotor speed coast down experiments with intermittent multiple shocks transmitted through test rig base. The test results demonstrate the reliability of the current rotor-bearing system to withstand external shock load excitations up to 30 g (pk-pk) delivered via the system foundation. The current research further evaluates the reliability of a rotor-hybrid gas bearing system to withstand base-transmitted load excitations. The investigation includes measurements of rotordynamic response on a rigid rotor supported on air FPTPBs, with an electromagnetic shaker introducing periodic load excitations through the test rig foundation, at various journal operating speeds and shaker excitation frequencies. The experimental results show that the test rotor-air bearing system has sufficient damping to suppress subsynchronous whirl motions, with frequencies locked at the test system natural frequencies, induced by periodic base load excitations.

## Literature Review: Rotor-bearing system response due to base or foundation motions

Modern turbomachinery such as compressors, turbines, and turbochargers can experience random or periodic load excitations or sudden imposed forces. Power plant turbines, for example, can be subjected to severe seismic vibrations. Turbochargers also usually experience random load excitations from uneven road surfaces, or periodic load excitations from engine vibrations, or shock loads from collisions. These excitations are transferred through foundations and mounts to the rotor-bearing system, and can induce serious damage caused by transient impact collision or rubbing contact between the rotors and stators such as bearings and seals. Therefore, it is necessary to analyze the reliability of the rotor-bearing systems utilized in critical rotating machines subject to external random or transient excitations prior to widespread application in industry.

Seismic excitation on large rotating machines is a typical example of random base load excitations (low frequency). In general, only an analytical investigation is selected for seismic analysis, since it is impractical and too costly to install excitation generating equipment. Srinivasan and Soni [9] review comprehensively the analysis methods for the dynamic forced performance of rotating machines under seismic excitations.

Samali et al. [10] and Kim et al. [11] present random vibration analysis of rotating machines subject to earthquake excitations using rigid and flexible rotor models. The random seismic base motion is modeled statistically using Monte Carlo simulation. A large number of Monte Carlo sample functions are required to obtain accurate statistical dynamic responses. The rotor dynamic response amplitude when using the flexible rotor model in Ref. [10] is larger than that derived from the rigid rotor model in Ref. [11]. Therefore, the flexible rotor model, often requiring a finite element approach, can guarantee a higher safety standard.

Kameswara Rao and Mirza [12] investigate analytically the dynamic performance of high-speed turbomachinery under earthquake excitations with a flexible rotor model. A modal analysis method, delivering conservative response results, is selected for calculating modal displacements and reaction forces at each mode. Modal responses are combined to obtain the total response. The analytical results demonstrate the rotor seismic response amplitudes are well within a design limit. Moreover, predicted

horizontal rotor displacements increase significantly when including pedestal masses and stiffnesses, yet the bearing reaction forces are not affected by this addition.

Gaganis et al. [13] analyze the performance of a rotor-bearing system subject to a large seismic excitation. The rotor-bearing system consists of a flexible rotor with a rigid disk in the mid span and supported on two nonlinear cylindrical fluid-film bearings. The rotor model is composed of 2-node beam finite elements. The equations of motion for the rotor-bearing system are obtained via Lagrange's equations. The bearing force coefficients are nonlinear functions of journal eccentricity, which is rather large due to the severe vibration amplitude caused by severe seismic excitations. For simplicity, the nonlinear bearing force coefficients are treated as piecewise linear and the model predicts more realistic results than purely linear bearing models when nonlinear mechanisms become significant. Suarez et al. [14] also develop a model of rotating machines under seismic excitations using the method in Ref. [13], but use a linear bearing model.

Many researchers perform predictions and experiments to determine the rotor response of a turbomachinery subject to external random or periodic motions, not limited to seismic excitations. Tessarzik et al. [15] study analytically and experimentally the rotor response of a turbogenerator to random and sinusoidal excitations. The rotor axial response to the external random vibrations is modeled as a linear three-mass system. The calculated and measured root mean square (RMS) axial response amplitudes agree well. The tested turbogenerator using gas hydrodynamic journal and thrust bearings runs at speed of 36 krpm, and experiences external random and single frequency vibrations with the acceleration of 5.4 g delivered by an electrodynamic shaker. The measured responses to sinusoidal and random excitations show a marked degree of similarity. Further, the response of the rotor-bearing system tends to behave as non-Gaussian distributions when increasing the external excitation level. This phenomenon indicates that the bearing gas film nonlinear characteristics become dominant at reduced film thickness, i.e., large journal eccentricities. Gaganis et al. [13] already resolved this issue as noted before.

Duchemin et al. [16] also conduct experiments on a flexible rotor-bearing system subject to single frequency base excitations. The external excitation is generated by an electromagnetic shaker mounted under the end of the test rig. The vertical acceleration is controlled within 0.75 g using the signal from an accelerometer for safety consideration,

since the test rig operates through the threshold speed of instability. The ball bearings in the experiment provide large damping to suppress the exponential increase of displacements at instability zones.

Using the same test rig setup in Ref. [16], Driot et al. [17] analyze, analytically and experimentally, the dynamic behavior of a base-excited flexible rotor. The theoretical model including two gyroscopic and parametrical coupled equations is derived using the Rayleigh-Ritz method. Based on the model, instability and normal forms analyses give the three instability zones and rotordynamic responses to external excitations. An electrodynamic shaker applies single frequency excitations to the test rig base. Measured rotor motion orbits exhibit excellent correlation with numerical results obtained from a classical time integration scheme.

Subbiah et al. [18] research analytically rotor responses due to random support excitations. The random base excitations are treated as Gaussian stationary and with a white noise of power spectral density type. The power spectral densities of rotor relative response amplitudes are determined using a modal analysis technique. The amplitude spectral density distributions of two rotor-bearing systems with flexible rotors supported on fluid-film bearings are investigated. The results show: a) cross-coupling effects from fluid-film bearings are significant in the calculated rotor response; b) rotational base excitations have no marked influence on the rotor lateral response.

Maruyama [19] analyzes the effects of engine-induced vibrations on the rotor response of a turbocharger. The tested turbocharger, with a shaft supported on an oil-lubricated semi-floating ring bearing, is installed on a 4-cylinder engine stand. The accelerations of the turbocharger center housing and compressor housing due to the engine vibrations are recorded along horizontal and vertical directions at 25%, 50%, and 100% of the full engine load. The recorded accelerations of the two housings, center and compressor, have frequency components at 300 Hz and 570 Hz, corresponding to the turbocharger support manifold natural frequencies.

Maruyama [19] also performs linear and nonlinear rotordynamic analyses of a commercial vehicle turbocharger shaft response including engine-induced housing excitations. The linear analysis involves the determination of system natural frequencies and corresponding rotor mode shapes along with the imbalance responses. The predicted

imbalance response amplitudes correlate well with those from measurements at high shaft speeds. Both of the predicted and tested response amplitudes increase with shaft speeds. The nonlinear analysis gives the subsynchronous shaft responses via a time transient computational scheme as the engine operating speed ranges from 1.0 krpm to 3.6 krpm. The nonlinear predicted and experimental results exhibit significant subsynchronous responses with similar amplitudes while the housing accelerations are introduced. Moreover, the engine-induced housing excitations tend to result in marked skewed shaft motion orbits. The comparisons of the predictions to experimental results validate the nonlinear analysis of rotordynamic behavior of a turbocharger involving engine-induced housing accelerations.

Transient shock loads are also important external excitations to rotor-bearing systems. Walton et al. [20] and Heshmat et al. [21] conduct shock load experiments on a small rotor-gas foil bearing test rig simulating a turbocharger or a turbojet. One end of the rig is raised to a certain height and dropped when the rotor runs at 100 krpm, and with bearing temperatures above 260°C. The bearing housing acceleration induced by shock load tests is approximate 40 g (pk-pk), larger than any to be faced under normal operating conditions. The rotor transient response amplitudes decrease quickly to a normal level amplitude in 75 ms. No rubbing contact or direct collision between the rotor and bearings happens in the shock load tests. The steady rotor response after transient loads demonstrates the robustness of withstanding externally shock excitations in the rotor-gas foil bearing system.

Lee et al. [22,23] develop a finite element model for a rotor-bearing system subject to base shock excitations and compare the predicted system transient response to experimental results. The flexible rotor supported on two ball bearings is modeled as several lumped mass elements connected with shaft elements. With the kinetic energy of the shaft and disk (lumped mass) elements, the equations of motion for these elements are derived using Lagrange's equations. The state-space Newmark method, due to its inherent numerical stability, is employed for direct time integration of the finite element system equations of motion. The base shock experiment includes an electromagnetic shaker delivering half-sine wave impacts, with magnitude of 3 g and a duration time of 10 ms, to a rotor test rig operating at a speed of 6.0 krpm. The test results reveal that the

rotor transient responses are affected by shock duration time. The predicted rotor transient responses agree well with the test data. Using a finite element analysis method, Jayson et al. [24,25] model the structure of a hard disk drive and investigate the dynamic response of a slider gas bearing, used for reading and writing data, subject to shock excitations.

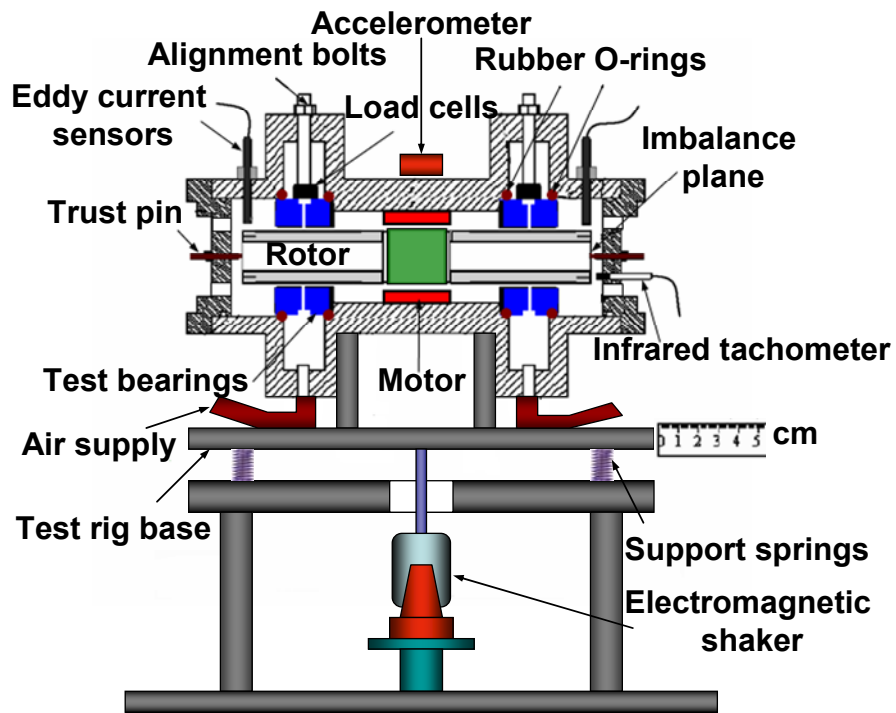
Ryu and San Andrés [8] conduct a comprehensive experimental work on the dynamic response of a rotor-bearing system subject to intermittent shock excitations, delivered from either an electromagnetic pusher or manually tilting and dropping off the whole test rig. The system consists of a rigid rotor supported on two hybrid gas bearings, flexure pivot tilting pad type. The shock loads, with maximum acceleration of 30 g (pk-pk) and frequency band up to 400 Hz, are transmitted to the test rig base while coasting down from 60 krpm. The bearings are fed with pressures equal to 2.36, 3.72, and 5.08 bar (ab). Note that the shock loads (100~400 N, pk-pk) excite both the natural frequencies of the rotor-bearing system (150-200 Hz) and the whole test rig (40 Hz). The resulting rotor response amplitude increases quickly up to 50  $\mu\text{m}$  (pk-pk) and recovers to normal amplitude level before impacts in 0.10 second, around 100 rotor revolutions when operating at 60 krpm. The recovery time still shows that the current rotor-hybrid gas bearing system has sufficient damping to dissipate the energy generated from sporadic shock excitations. The exponential decay of the shaft speed while coasting down denotes viscous drag type during the shock load experiments. The tests show no rubbing contact or direct collision between the rotor and bearings. The experimental results lend credence to the good shock load withstanding characteristics of the rotor-hybrid gas bearing system.



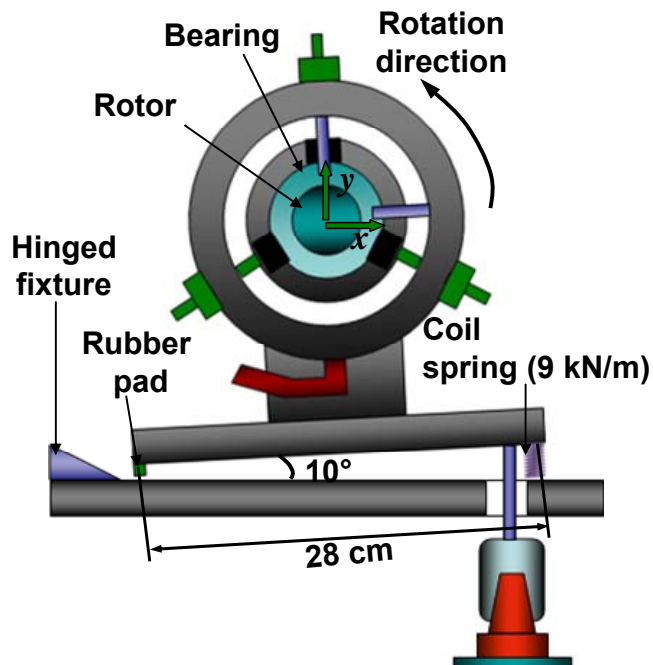
## Description of Experimental Facility

Figure 1 depicts schematic front and side views of the test rig for evaluating the dynamic forced response of a rotor-hybrid gas bearing system subject to (external) base or foundation motions induced by an electromagnetic shaker. Figure 2 shows a photograph of the test rig including some instrumentation. A brushless AC motor (max. speed 99 krpm) drives the rotor supported on two flexure pivot, tilting pad hydrostatic gas bearings. Table 1 details major dimensions of the test rotor and bearings.

The test rig base comprises of a thick plate and two bearing housings connected to a main cylindrical body containing the stator armature of the electric motor. The overall weight of the test system including bearings and rotor is ~48 kg. The whole test rig rests on a table; a hinge restrains one side of the base plate. Two coil springs (stiffness of 9,000 N/m) support the other side of the base plate at its ends, see Fig. 1 (b). The whole test rig can tilt (rotate) around the hinged fixture (static angle of  $10^\circ$ ). An electromagnetic shaker, mounted under the test table, delivers forced excitations to the base plate through a push rod, not rigidly affixed to the test rig. A piezoelectric accelerometer (5 mV/g) affixed atop the test rig main body can record the shaker-induced motions.



(a) Side view



(b) Axial view

Fig. 1 Schematic views of hybrid gas bearing test rig modified with shaker (not to scale) to induce base motion excitations (unit: cm).

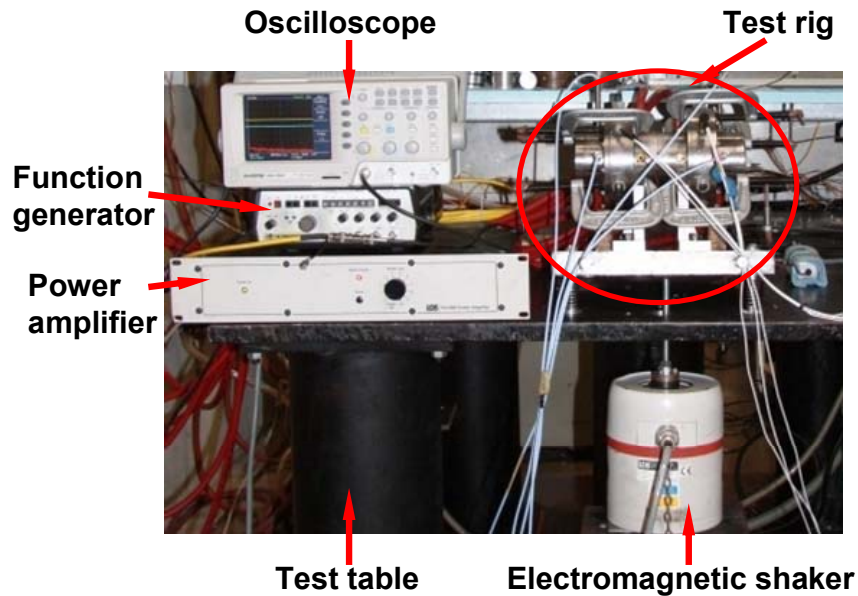


**Fig. 2 Photograph of test rig with connection to shaker and instrumentation**

**Table 1 Main parameters of test rotor and flexure-pivot tilting-pad bearings**

<b>Parameter</b>	<b>Magnitude</b>	<b>Unit</b>
Rotor mass, $m$	0.825	kg
Rotor length, $L$	190	mm
Rotor diameter, $D_r$	$28.56 \pm 0.003$	mm
Bearing diameter, $D_b$	$28.64 \pm 0.013$	mm
Bearing axial length	33.2	mm
Radial clearance, $C_b$	$42 \pm 8$	$\mu\text{m}$
Pad arc length	72	degree
Pivot offset	60%	
Preload	0.4	
Web thickness	2	mm
Orifice diameter	0.5	mm
Pad inertia	$3.56 \times 10^{-7}$	$\text{kg m}^2$
Pad rotational stiffness	62	N m/rad

Figure 3 depicts the test rotor, 190mm in length, 28.56mm in diameter, and 0.825kg in mass. The rotor consists of a steel shaft (15mm in diameter), a motor armature, and two bearing sleeves. The rotor surface at the two bearing positions is coated with hard-chrome (thickness  $0.254 \pm 0.025$  mm) to reduce friction. The rotor end plane contains eight 1mm holes,  $45^\circ$  apart, and into which known masses can be inserted for imbalance

response measurements. The first free-free elastic mode of the rotor is measured at  $\sim 115$  krpm [6], well above the maximum operating speed of the test rig (99 krpm). Therefore, the rotor can be regarded as a rigid body for later analysis. The bearing supports and rotor displacement measurement positions are also shown in the photograph.

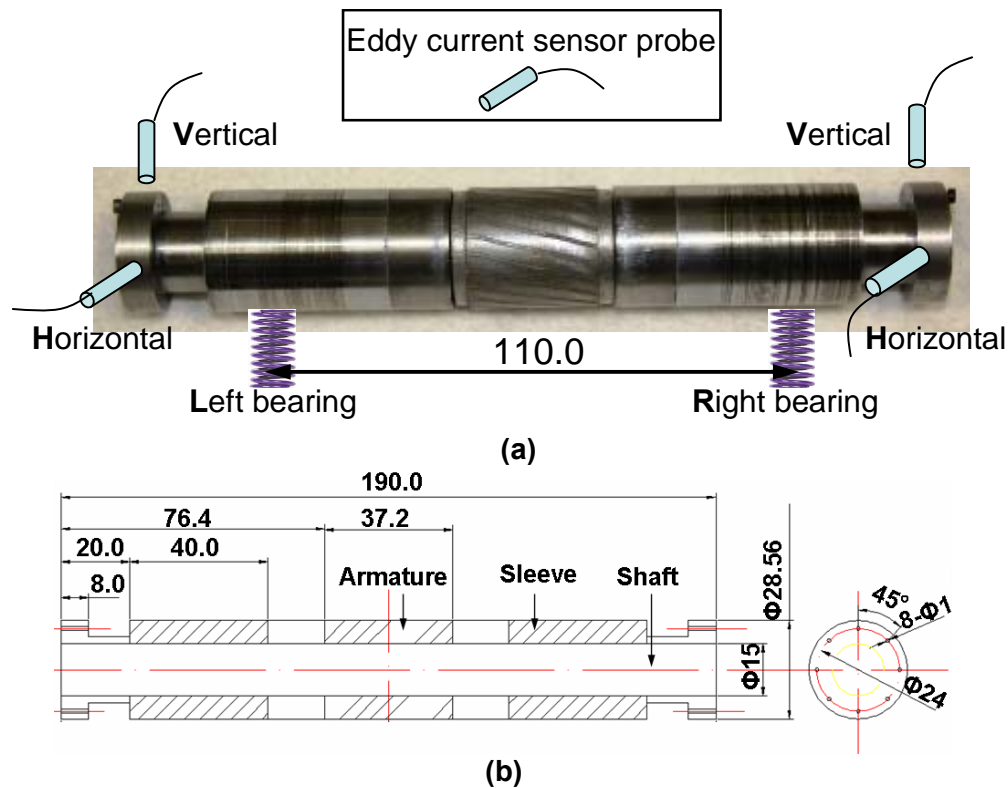


**Fig. 3 Photograph (a) and schematic view (b) of rotor (unit: mm). Location of displacement sensors and bearings noted.**

Figure 4 shows a test hybrid flexure-pivot tilting-pad gas bearing (FPTPB). Three alignment bolts,  $120^\circ$  apart, position each test bearing within its housing. Each bearing, made of beryllium copper (BeCu), has four  $72^\circ$  pads with 60% offset supported on thin webs, 2 mm thickness. Radial holes, 0.5 mm diameter, are machined through each web to supply pressurized air directly into each bearing pad. Teflon<sup>®</sup> coating (thickness 0.005 mm) is applied onto the pad surface to reduce friction while at rotor start-up and shut down. Upon assembly, a side cap and O-rings enclose a test bearing in its housing. Special care in the assembly is needed to ensure there is no air leaking through the O-rings.

The current bearing nominal clearances ( $42 \pm 8 \mu\text{m}$ ) are uniform circumferentially. Since the test rig supported on the coil springs is tilted statically by  $10^\circ$  (see Figure 1), the current configuration is not load-on-pad (LOP), see the coordinate and static load direction in Fig. 4. Appendix C details the predicted gas bearing stiffness and damping force coefficients derived with the model in Ref. [5].

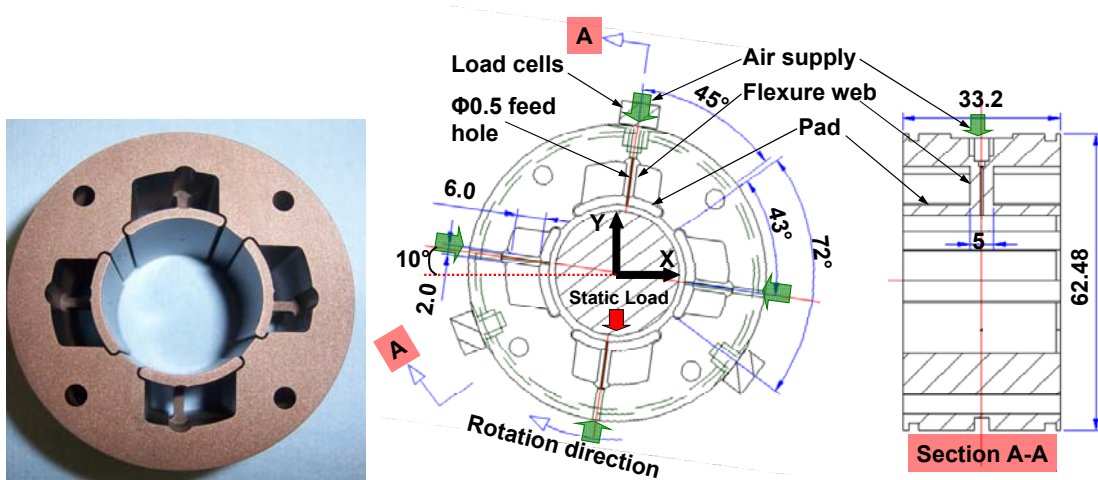


**Fig. 4 Photograph and drawings of test hybrid flexure-pivot tilting-pad gas bearing. Noted coordinate system (X: horizontal, Y: vertical) (units: mm)**

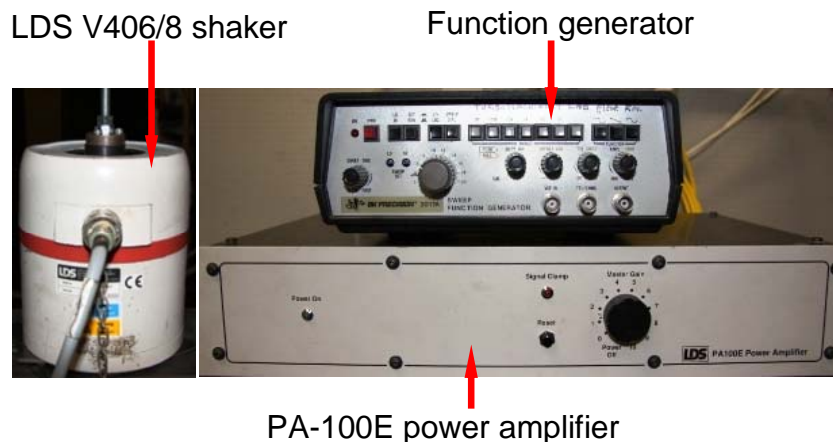
Three piezoelectric load cells, each between the bearing outer diameter and an alignment bolt, aim to measure transmitted dynamic forces to the test rig bearing housing. However, since the side cap and O-rings push on the bearing side, these elements take an unknown part of the bearing reaction forces. Hence, the recorded forces are smaller than the actual bearing forces.

At each end of the rotor, two eddy current sensors, orthogonally positioned along the vertical (V) and horizontal (H) directions shown in Fig. 3 (a), measure the rotor motion amplitudes. Table 2 presents the sensitivities of the force and displacement sensors [1]. An infrared tachometer mounted to the right side cover of the test rig, serves as a keyphasor signal for data acquisition. In addition, two turbine flow meters, uncertainty of  $\pm 0.05 \text{ L/min}$ , measure mass flow rate into the test bearings. Refs. [1,6,7,8] also detail the test rig components.

**Table 2 Sensitivities of sensors [1]**

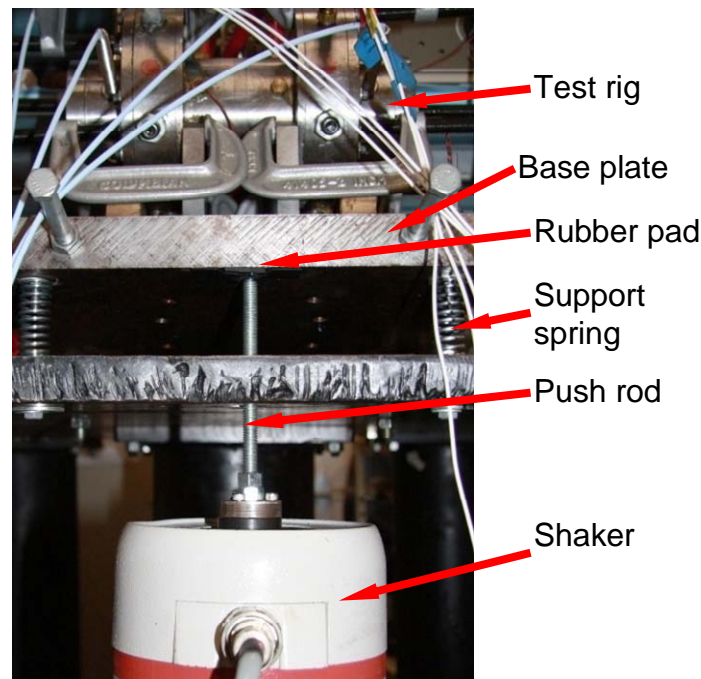
Sensor	Location	Sensitivity	Unit
<b>Load cell</b>	Left bearing	119	mV/N
	Right bearing	120	mV/N
<b>Eddy current sensor</b>	Left vertical (LV)	8.5	mV/ $\mu$ m
	Left horizontal (LH)	8.6	mV/ $\mu$ m
	Right vertical (RV)	8.7	mV/ $\mu$ m
	Right horizontal (RH)	8.6	mV/ $\mu$ m
<b>Accelerometer</b>	Top of main body of test rig	5	mV/g

Figure 5 shows the electromagnetic shaker (LDS V406/8) with power amplifier (PA-100E) supplying maximum output power of 147 W and a function generator (BK PRECISION 3017A). The electromagnetic shaker weighing 14.1 kg has a resonance frequency at 9 kHz. The shaker can deliver excitation forces up to 98 N with an adjustable frequency ranging from 5 Hz to 9 kHz. At low frequencies (~less than 20 Hz), the shaker stroke can be as large as 14.0 mm. At frequencies higher than 50 Hz, the shaker can produce maximum acceleration up to 50 g. A function generator provides wave type signals at diverse frequencies to the power amplifier, which delivers the amplified signals to the shaker. The periodic load excitations from the shaker are transferred to the test rig base plate through a steel push rod, 13cm in length and 9.2cm in diameter. The rod connecting the shaker to the base plate is not affixed rigidly to the test rig base. The rod merely pushes on the base plate!



**Fig. 5 Photograph of electromagnetic shaker (LDS V406/8) with power amplifier (PA-100E) and function generator**

Figure 6 presents a close up photograph of the shaker and test rig base plate and the push rod connecting element. The test rig is softly supported on the coil springs. The measured natural frequency of the whole test rig on the coil springs is just 5 Hz. Appendix A presents results of impacts delivered on the test rig and demonstrating a natural frequency at ~5 Hz. Since the steel rod is not affixed rigidly to the test rig base plate, for shaker induced excitations with frequencies above the low natural frequency of 5 Hz, the base plate collides intermittently with the push rod. That is, above this threshold frequency, the push rod and base plate can at times be apart and then become suddenly in contact. To soften the impacts, and in order to protect the shaker mainly, a thin rubber pad (thickness 2 mm) is glued to the base plate at the location where the rod pushes.



**Fig. 6 Photograph of connection of shaker to test rig base plate**

## **Description of Experimental Procedure**

In the experiments, both gas bearings (Left and Right) are supplied with a constant supply pressure at 2.36, 3.72 or 5.08 bar (ab). Rotor speed coast down tests from 35 krpm are conducted with the rotor as best balanced as possible, i.e. a baseline condition. First, measurements without the shaker exciting the test rig are obtained. Next, the shaker is active and the power amplifier supplies single frequency signals at 5, 6, 9, and 12 Hz.



The shaker delivers periodic type load excitations to the rig foundation during the rotor speed coast down tests. Refer to Fig. 3 (a) for the disposition of the bearings and sensors for rotor response measurements.

Recall that the natural frequency of the whole test rig with its base supported on the soft coil springs is  $\sim 5$ Hz. At this frequency, small external loads cause large displacements (bouncing) of the whole test rig. Hence, the shaker load magnitude at 5 Hz is smaller than those at the other three frequencies to ensure safe operation of the test system. The shaker load excitation amplitudes at 6, 9, and 12 Hz are identical.

In addition to the coast down tests, rotordynamic measurements at fixed rotor speeds (26, 30, and 34 krpm) are conducted with the shaker delivering load excitations at frequencies equal to 5, 6, 9, and 12 Hz. The gas supply pressures into the bearings are fixed at 2.36, 3.72, and 5.08 bar (ab) during each test.

The rotor responses are recorded in both time and frequency domains using an in-house built LabVIEW® program. The measurements include rotor speed, test rig base acceleration, rotor displacements at the ends of the rotor, and bearings' transmitted forces. The sampling size and sampling rate are 2,048 and 10,000 samples/s, respectively. During rotor speed coast down tests, the system acquires data records when the rotor speed changes by 500 rpm.

The objective of the measurements is to quantify the effects of base acceleration (amplitude and frequency), and rotor speed and bearings' feed pressure, on the amplitude of rotor motion response. Ultimately, the measurements intend to demonstrate the reliability of the test rotor-air bearing system to withstand external periodical base excitations.

## **Experimental Results**

### **Typical base motion induced accelerations**

Figures 7 and 8 show the measured rig base accelerations due to the shaker induced load excitations with a frequency of 6 Hz, when the rotor is turning at 34 krpm. Figure 7 shows the acceleration in time domain, and Fig. 8 depicts the FFT (Fast Fourier Transform) of the acceleration signal. Note that the accelerometer is affixed atop the motor casing of the test rig, see Fig. 1 (a). Recall that the periodic input excitations from



the shaker in actuality transfer impacts to the rig base, thereby rendering many frequency components excited, as shown in Fig. 8. The base acceleration shows harmonic frequencies with significant amplitudes, in particular at two, three and four times the shaker excitation frequency. In the time domain, the peak delivered acceleration is 1.7 g. In the frequency domain, the peak amplitude, approximately 0.2 g, corresponds to the fundamental excitation frequency of 6 Hz.

The acceleration components at 51 Hz and 624 Hz with distinctive amplitudes,  $\sim 0.1g$  and  $\sim 0.2g$ , are caused by the electric motor. These two frequency components do not appear when the electric motor is turned off.

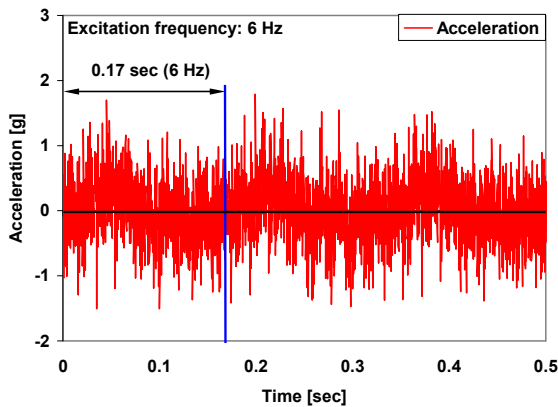


**Fig. 7 Typical measured base acceleration in time domain. Shaker excitation frequency: 6 Hz. Rotor speed = 34 krpm (567 Hz)**

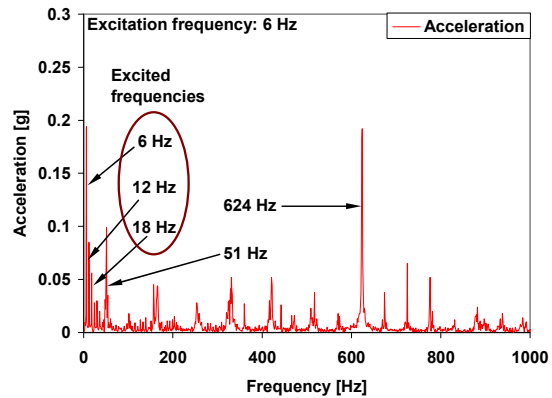


**Fig. 8 Typical measured base acceleration in frequency domain. Shaker excitation frequency: 6 Hz. Rotor speed = 34 krpm (567 Hz)**

Figure 9 shows the frequency content (FFT) of the test rig base accelerations induced by shaker excitations at main frequencies of 5, 6, 9, and 12 Hz. Harmonics of the main excitation frequency are apparent. The frequency spectra shown are up to 100 Hz only for illustrative purposes. The measured base accelerations have similar amplitudes and frequency content above 100 Hz for the various excitation frequencies.

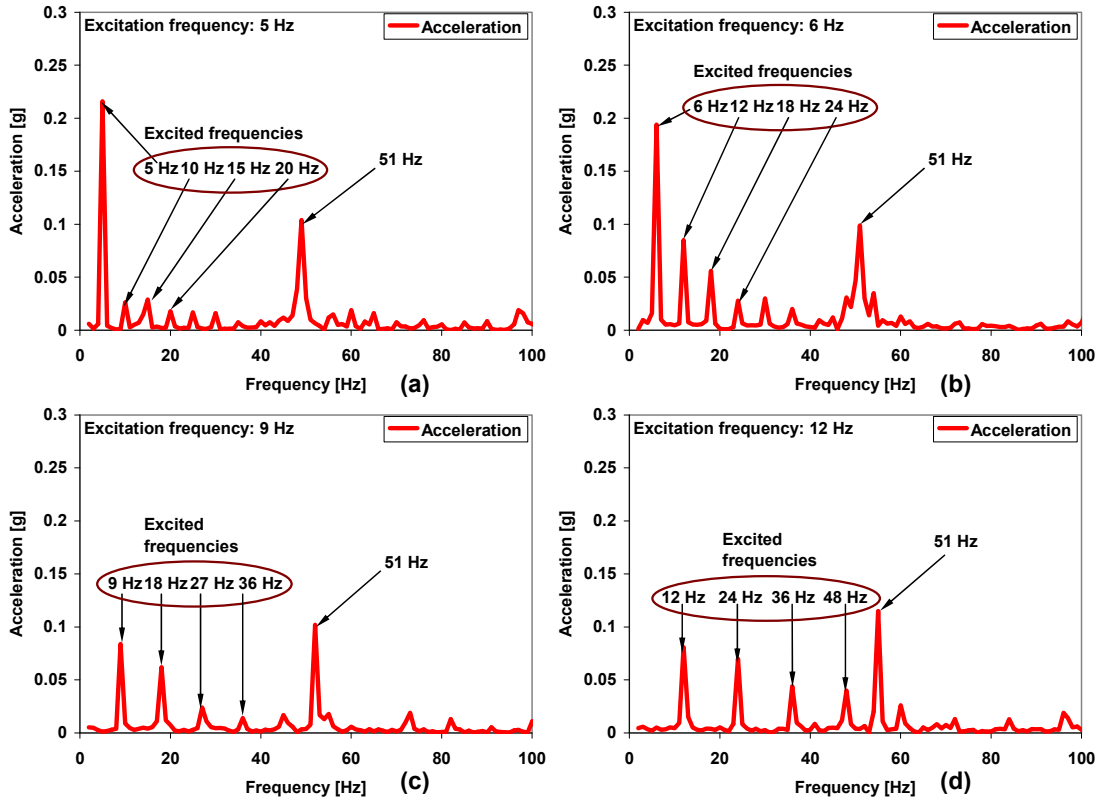


**Fig. 9 Typical measured base acceleration in frequency domain. Shaker excitation frequencies: (a) 5 Hz; (b) 6 Hz; (c) 9 Hz; (d) 12 Hz. Rotor speed = 34 krpm (567 Hz)**

### Rotor speed coast down tests

Figures 10 and 11 show the slow roll compensated rotor synchronous response amplitudes recorded at the left rotor end and right rotor end, along the vertical direction, (LV and RV). The figure includes tests with the gas bearings supplied at various feed pressures: 2.36, 3.72 and 5.08 bar (ab). There is no shaker forced excitations introduced into the test rig. In the measurements, the rotor spins at 35 krpm and coasts down with the motor turned off.

The rotor speeds at which motion amplitudes peak correspond to system natural frequencies at the respective bearing supply pressures [26]. In general, the bearing feed pressure increases the system natural frequencies and peak amplitudes [4]. The system fundamental natural frequency for each bearing feed pressure condition is labeled in the figures. These natural frequencies will be compared to those frequencies excited when the active shaker induces base load excitations.

At low rotor speeds, below 8 krpm, sudden rubs and contact with rapid deceleration between the rotor and its bearings leads to the irregular responses, as shown in Figs. 10 and 11. Appendix B shows the rotor speed versus time during the coast downs and with the shaker active and the gas bearings supplied with various feed pressures.

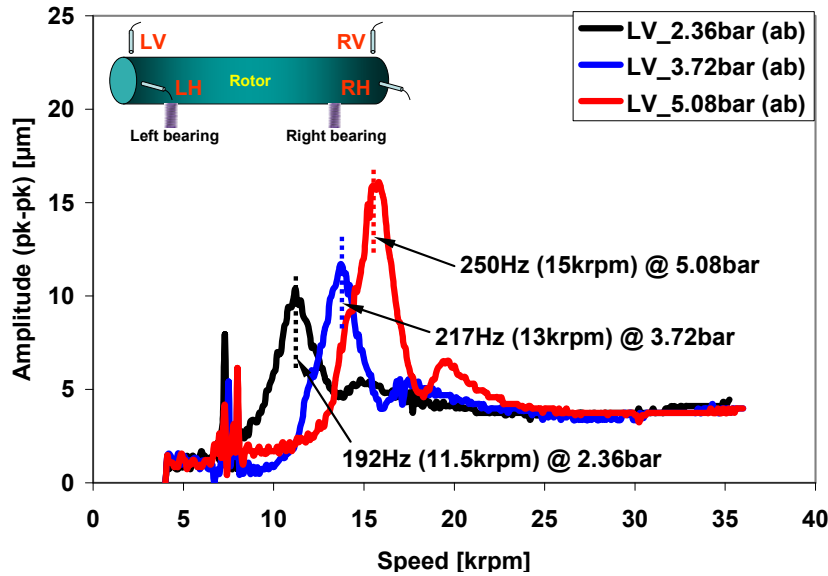


Fig. 10 Peak-peak amplitude of rotor synchronous response during rotor speed coast down from 35krpm. Slow roll compensated measurements at rotor left end, vertical direction (LV). No shaker induced excitation. Bearing feed pressures: 2.36, 3.72, and 5.08 bar (ab).

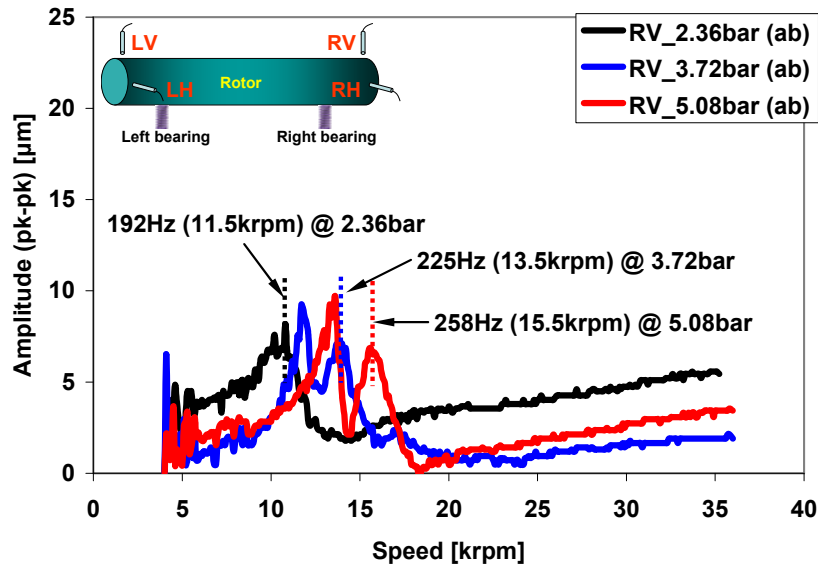


Fig. 11 Peak-peak amplitude of rotor synchronous response during rotor speed coast down from 35krpm. Slow roll compensated measurements at rotor right end, vertical direction (RV). No shaker induced excitation. Bearing feed pressures: 2.36, 3.72, and 5.08 bar (ab).

Figures 12 through 15 show waterfall plots of rotor motion response recorded at the left and right rotor ends along the vertical direction (LV & RV). The rotor speed coasts down from 35 krpm to 2 krpm and the gas bearings are supplied with feed pressure at 2.36 bar (ab). Figures 12 and 14 present results without base induced motions. Figures 13 and 15 depict measurements with shaker excitations at 12 Hz. See Fig. 9 (d) for the test rig base accelerations. In the waterfalls, the horizontal and vertical axes show the frequency and amplitude of the rotor motions. The third axis (into the page) represents the rotor speed.

Without base excitation, as depicted in Figs. 12 and 14, the only significant response components are at the rotor synchronous frequency and its second harmonic. Subsynchronous motions of insignificant amplitude appear for rotor speeds above 30 krpm. Note that the synchronous response amplitude along the LV direction is smaller than that along the RV direction.

With base excitation (shaker at 12 Hz), as shown in Fig. 13, rotor LV motions with two fixed frequencies appear. The 24 Hz component equals twice the main excitation frequency of 12 Hz, depicted in Fig. 9 (d). The motion component at 193 Hz corresponds to the natural frequency of the rotor-bearing system when operating with bearing feed pressure equal to 2.36 bar (ab). See Figs. 10 and 11 for the critical speeds. Note that along the RV direction, the rotor motions show a frequency component with the natural frequency only, as shown in Fig. 15.

Even though the 12 Hz shaker load excitation induces subsynchronous whirl at the system natural frequency, the dominant response is still synchronous. That is, the measurements do not show rotordynamic instability.

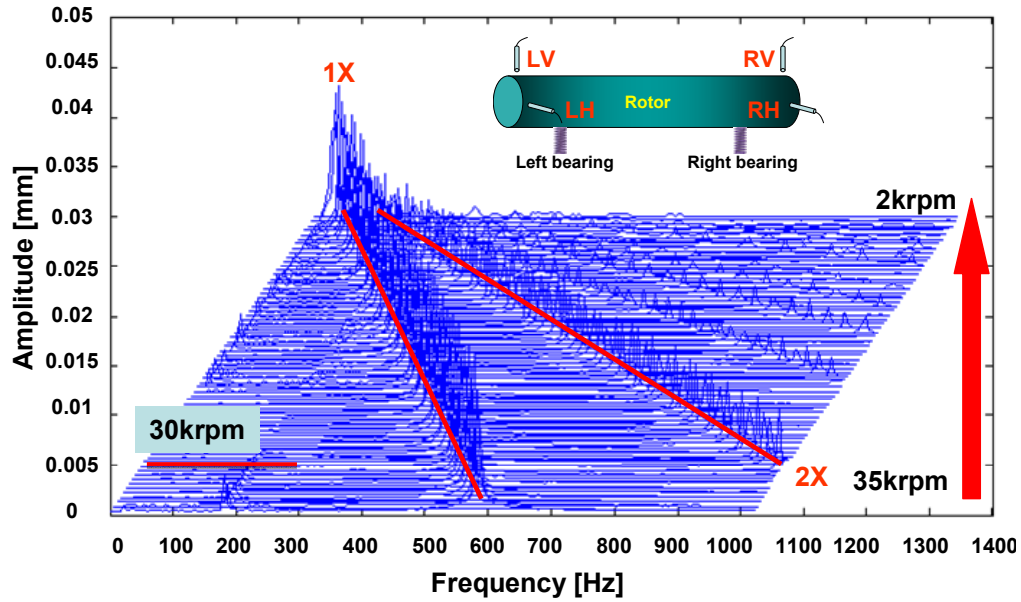


Fig. 12 Waterfall of rotor motions measured at left end, vertical direction (LV). No base excitation. Bearing feed pressure: 2.36 bar (ab).

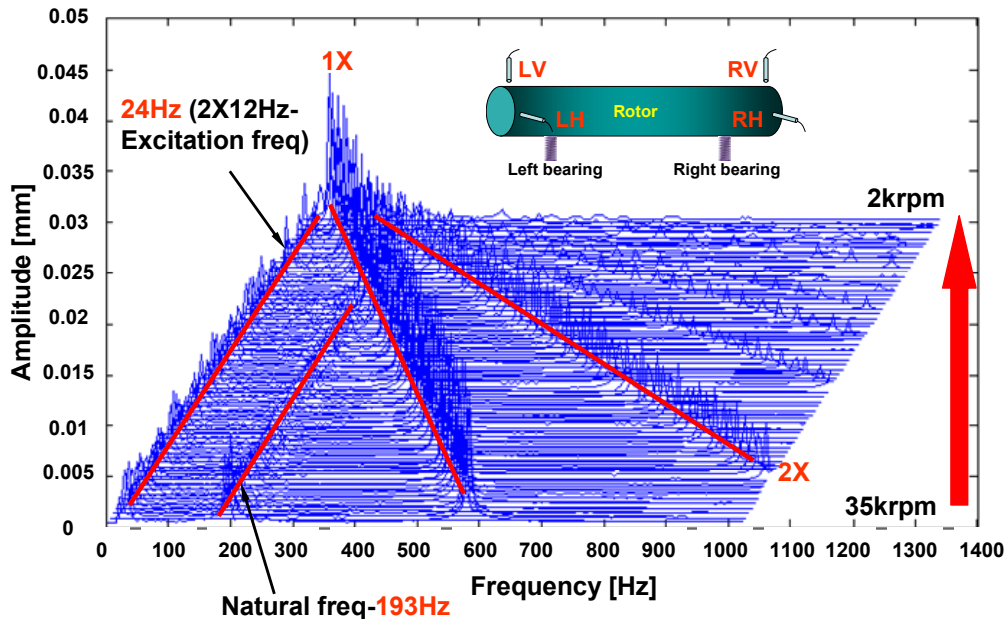
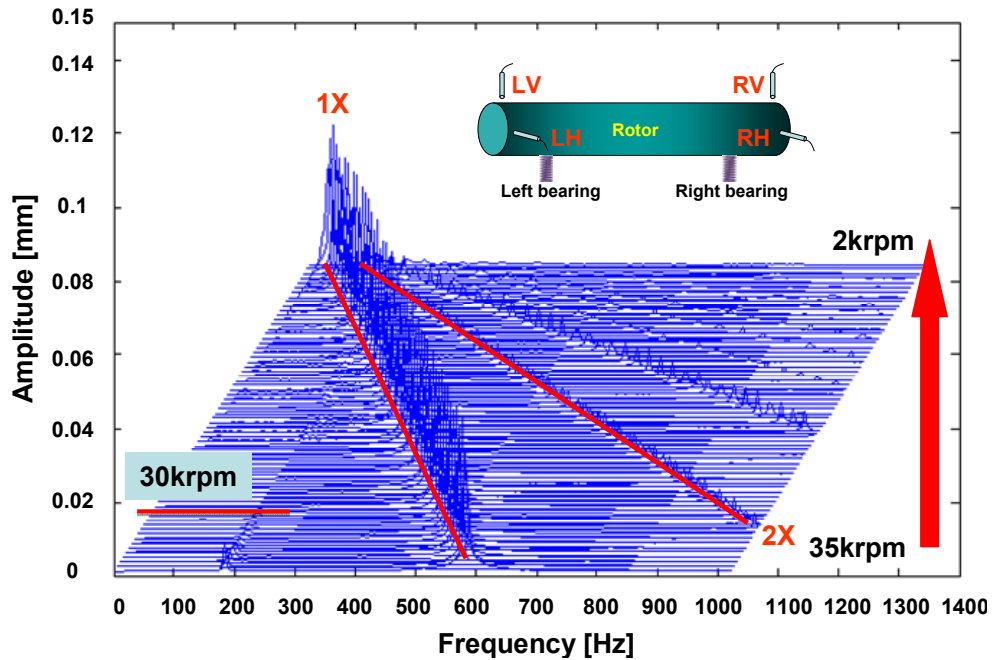
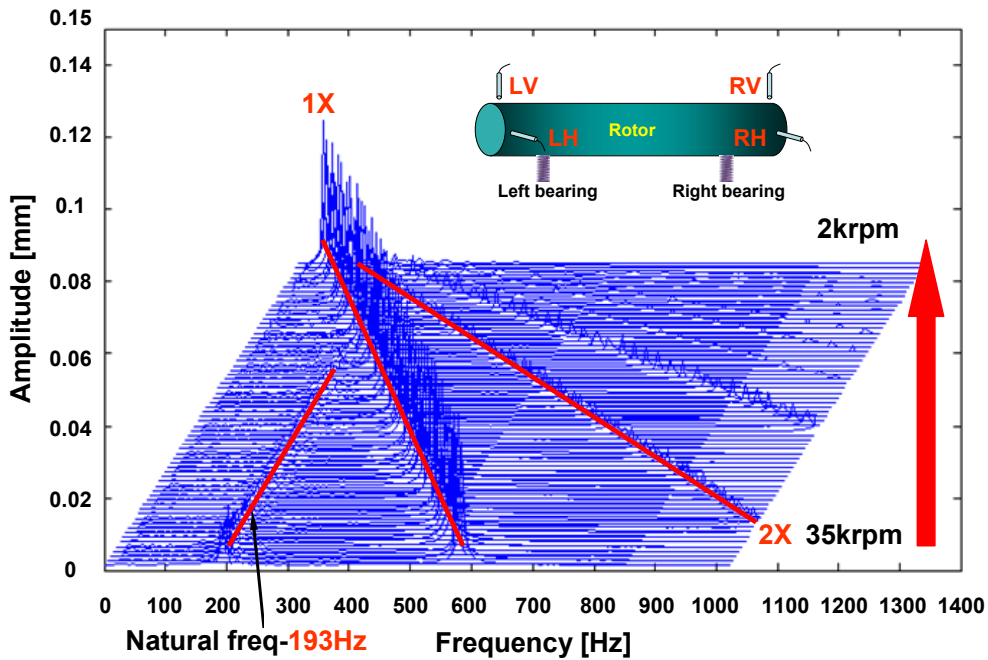


Fig. 13 Waterfall of rotor motions measured at left end, vertical direction (LV). Base excitation with main frequency at 12 Hz. Bearing feed pressure: 2.36 bar (ab).



**Fig. 14** Waterfall of rotor motions measured at right end, vertical direction (RV). No base excitation. Bearing feed pressure: 2.36 bar (ab).



**Fig. 15** Waterfall of rotor motions measured at right end, vertical direction (RV). Base excitation with main frequency at 12 Hz. Bearing feed pressure: 2.36 bar (ab).

Post processing of the waterfall data renders the whirl frequencies and associated amplitudes of rotor motion, as shown in Figures 16 and 17 for measurements at the left end, and in Figures 18 and 19 for measurements at the right end, both along the vertical

direction. The data corresponds to base excitation with main frequency at 12 Hz. The gas bearings are supplied with 2.36 bar (ab). Only synchronous and subsynchronous frequency components are reported. The measurements show little effect from base excitations on supersynchronous responses, see Figs. 12 through 15.

In Fig. 16, the main frequency components of rotor motion are synchronous (1X), and at the system natural frequency 192 Hz, and at 24 Hz, i.e. twice the fundamental base excitation frequency. The subsynchronous components, at 24 Hz and 192 Hz, show smaller amplitudes compared to the synchronous ones. Along the right end vertical direction (RV), the rotor response whirl frequency and amplitude components, see Figs. 18 and 19, show only the system natural frequency and not the 24 Hz component. Note that the rotor response along the RV direction has larger amplitudes than the rotor response along the LV direction.

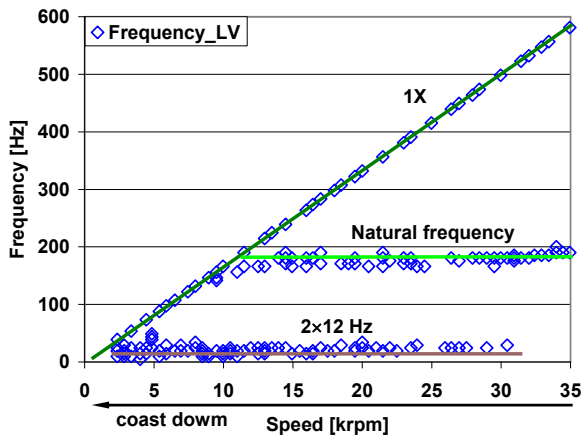


**Fig. 16 Whirl frequency versus rotor speed for measurements at left end, vertical direction (LV). Shaker induced excitation frequency: 12 Hz. Bearing feed pressure: 2.36 bar (ab).**

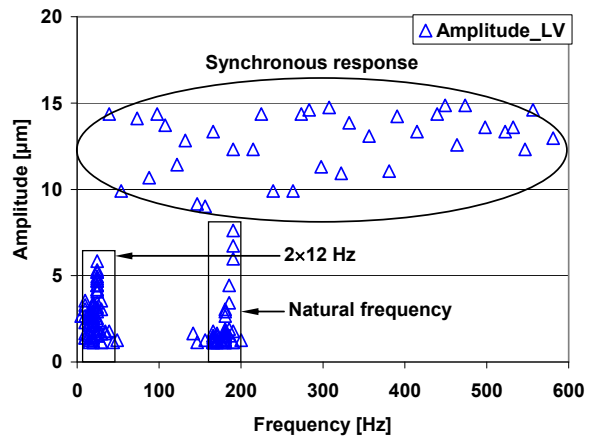


**Fig. 17 Amplitudes of rotor motion versus rotor speed for measurements at left end, vertical direction (LV). Shaker induced excitation frequency: 12 Hz. Bearing feed pressure: 2.36 bar (ab).**

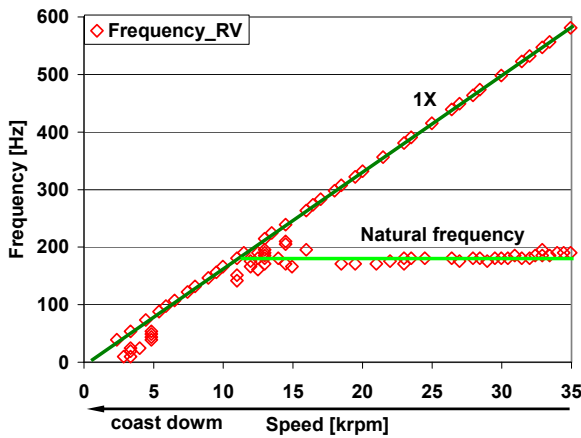


**Fig. 18 Whirl frequency versus rotor speed for measurements at right end, vertical direction (RV). Shaker induced excitation frequency: 12 Hz. Bearing feed pressure: 2.36 bar (ab).**

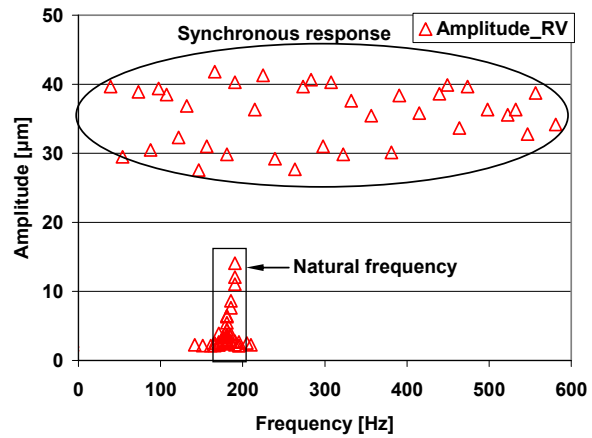


**Fig. 19 Amplitudes of rotor motion versus rotor speed for measurements at right end, vertical direction (RV). Shaker induced excitation frequency: 12 Hz. Bearing feed pressure: 2.36 bar (ab).**

**[Rotor motion response at a fixed rotor speed and increasing supply pressures into gas bearings](#)**

Figures 20 and 21 depict the FFT amplitude of rotor displacements for operation at a fixed rotor speed (34 krpm) while the gas bearings are supplied with increasing pressures at 2.36, 3.72, and 5.08 bar (ab). The measurements are at the left and right ends of the rotor, vertical direction. The shaker excitation frequency is fixed at 12 Hz. For the same test conditions, Figures 22 and 23 show the FFT of the transmitted (vertical) bearing forces, left (LV) and right (RV). For illustrative purposes, the figures show the curves offset an arbitrary value to make more distinctive the influence of bearing feed pressure on the rotor response.

Since the rotor speed is well above the system natural frequency, gas supply pressure into the bearings has little effect on the amplitude of synchronous rotor response, see Fig. 10. The rotor displacements also show whirl motions with frequency components at twice the excitation frequency, a frequency component ranging from 70 Hz to 90 Hz, and the system natural frequency. Recall that the system natural frequencies are 193 Hz, 215 Hz, and 243 Hz for operations with bearing feed pressures of 2.36, 3.72, and 5.08 bar (ab), respectively. These frequencies correlate well with those obtained from the rotor



synchronous response amplitudes, see Figs. 10 and 11. The base induced motions of the test rotor (at 24 Hz) appear to increase slightly with supply pressure into the bearings. Most important, however, is to realize that for the largest feed pressure (5.08 bar) the rotor does not show excitation of its natural frequency. That is, the test system appears to have more damping at high rotor speed than the coast down tests show, see Figure 10. The rotor displacement along the RV direction, see Fig. 21, shows excitation of the rotor-bearing system natural frequency in addition to the synchronous frequency component.

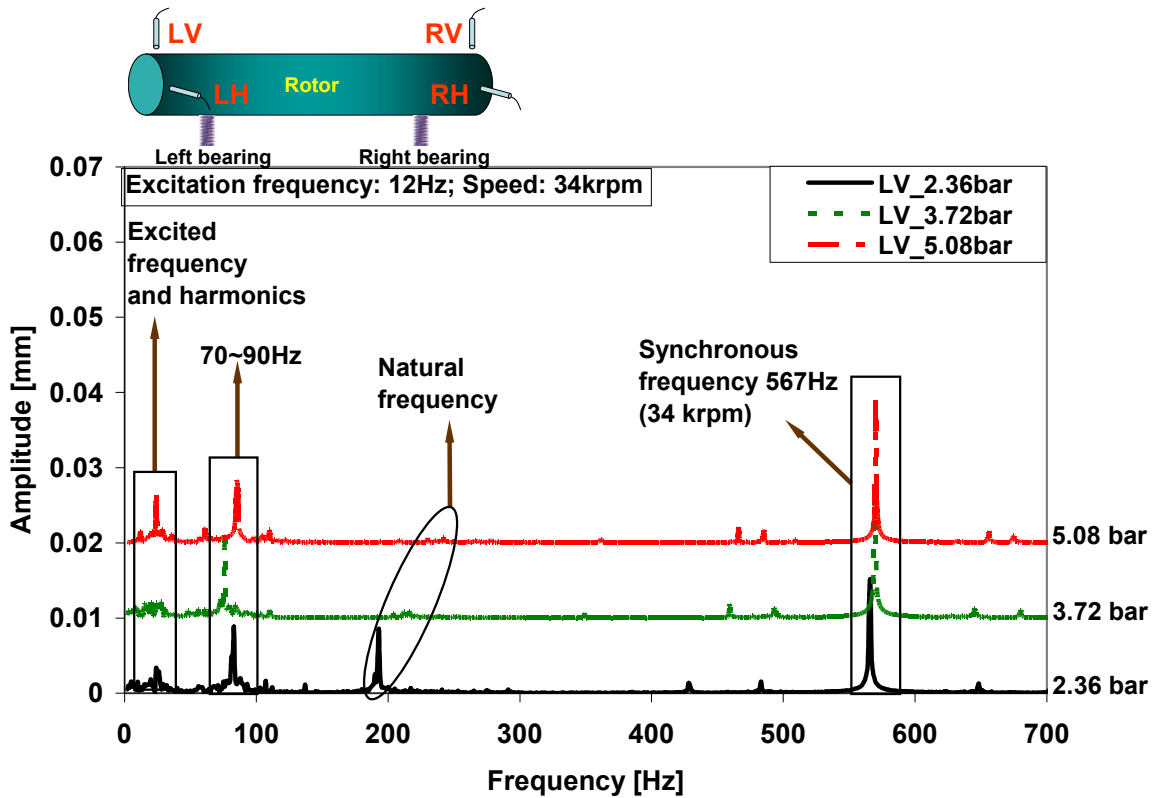
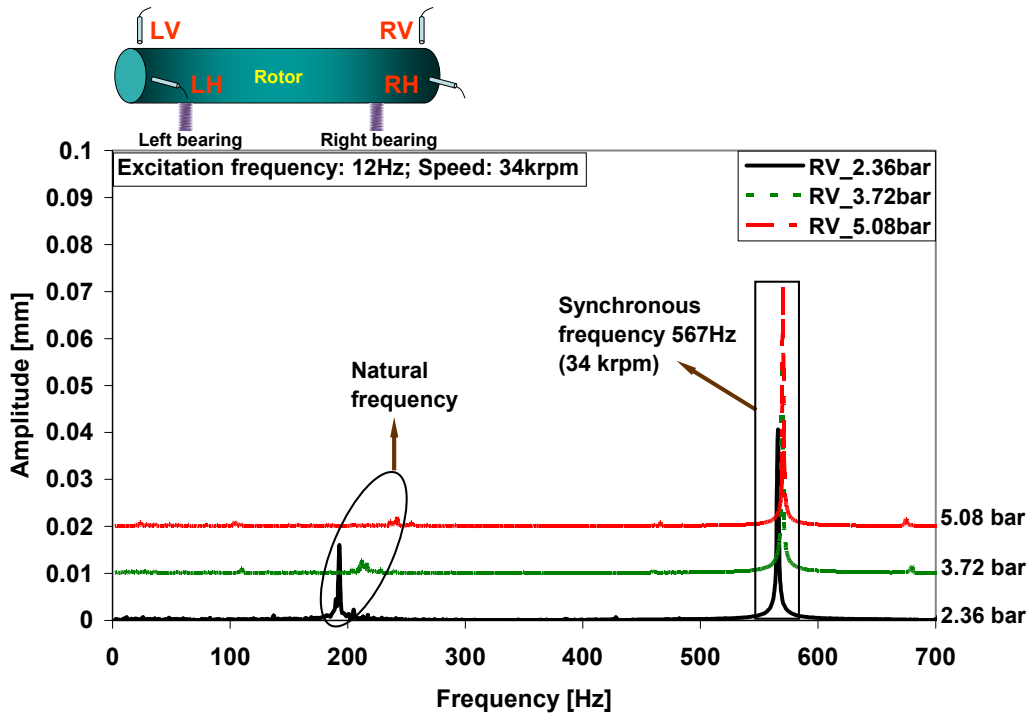


Fig. 20 FFT amplitudes of rotor displacement measured at left end, vertical direction (LV). Fixed rotor speed at 34 krpm (567 Hz) and shaker induced excitation frequency at 12 Hz. Bearing feed pressures: 2.36, 3.72, and 5.08 bar (ab).



**Fig. 21 FFT amplitudes of rotor displacement measured at right end, vertical direction (RV). Fixed rotor speed at 34 krpm (567 Hz) and shaker induced excitation frequency at 12 Hz. Bearing feed pressures: 2.36, 3.72, and 5.08 bar (ab).**

The bearing transmitted forces shown in Figures 22 and 23 correspond to measurements with the vertical load cell installed in each bearing casing. These loads are not the actual vertical component of the bearing force because there are two other load cells located 120°CW and 120°CCW, as shown in the graphs. In addition, the bearing side caps and rubber O-rings transmit an unknown part of the bearing actual reaction forces. The forces show components at the input excitation frequency of 12 Hz and its harmonics (24 Hz and 36 Hz). The frequency component at 70~90 Hz, apparent in the rotor displacement along the LV direction in Fig. 20, does not appear in the measured bearing forces. Most importantly, note the large amplitude at the system natural frequency, exacerbated as the bearing supply pressure decreases.

In the measured rotor displacement amplitudes with base excitations, shown in Figs. 20 and 21, amplitude components at the rotor-bearing system natural frequency are smaller than those amplitudes at the synchronous frequency. However, in the bearing forces, the components at the rotor-bearing system natural frequency have dominant amplitudes, as shown in Figs. 22 and 23. Therefore, when the rotor response exhibits

apparent subsynchronous motions at the system natural frequency, the bearing reaction forces at these natural frequencies are dominant, in particular when the gas bearings are supplied with low feed pressures.

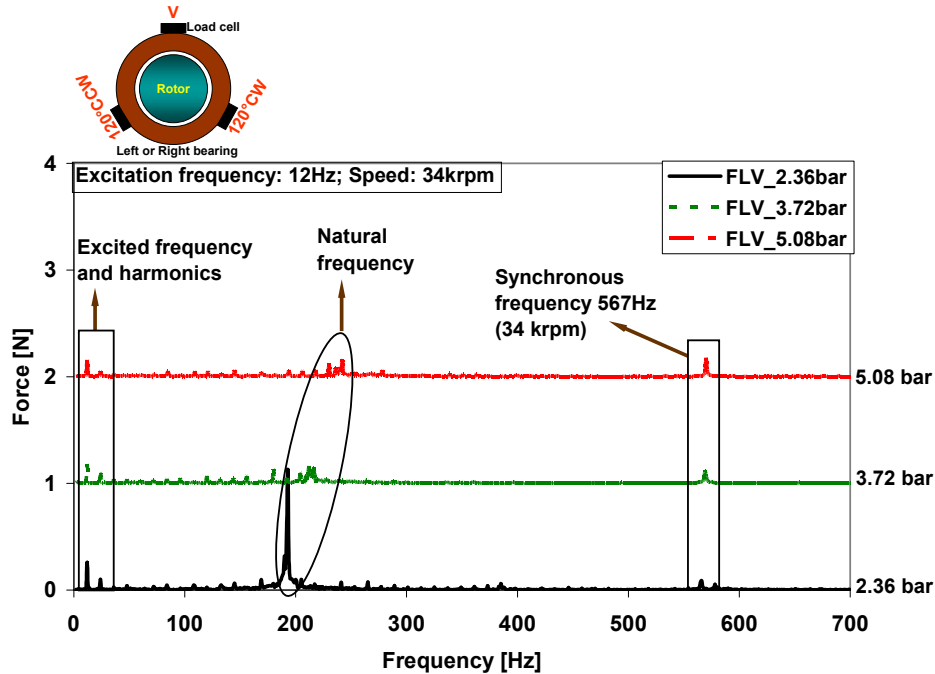


**Fig. 22** FFT amplitudes of left bearing force, load cell in vertical direction (FLV). Fixed rotor speed at 34 krpm (567 Hz) and shaker induced excitation frequency at 12 Hz. Bearing feed pressures: 2.36, 3.72, and 5.08 bar (ab).

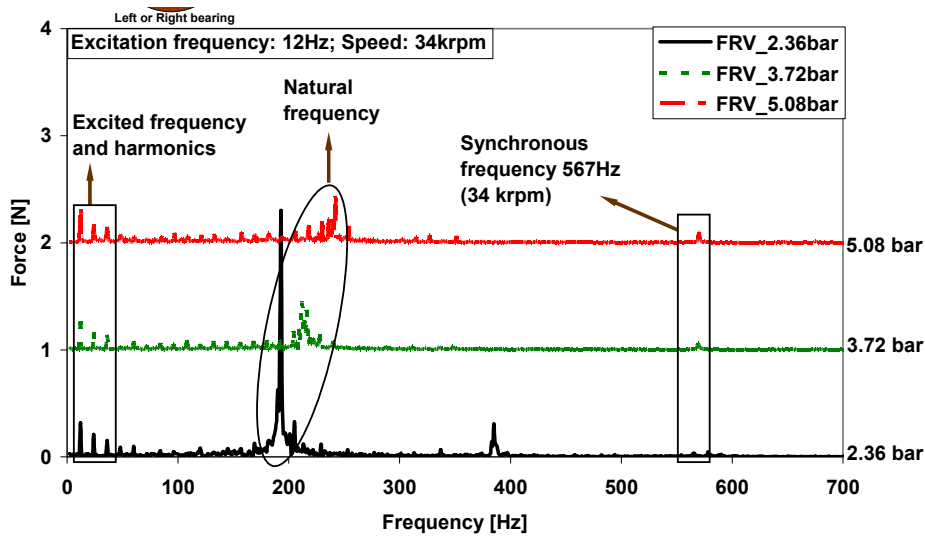


**Fig. 23** FFT amplitudes of right bearing force, load cell in vertical direction (FRV). Fixed rotor speed at 34 krpm (567 Hz) and shaker induced excitation frequency at 12 Hz. Bearing feed pressures: 2.36, 3.72, and 5.08 bar (ab).

## **Rotor motion response at a fixed feed pressure into gas bearings and three rotor speeds**

Figures 24 and 25 depict the FFT amplitude of rotor displacements for operation at three rotor speeds equaling 26, 30, and 34 krpm. The gas bearings are supplied with feed pressure at 2.36 bar (ab). The measurements are at the left and right ends of the rotor, vertical direction. The shaker excitation frequency is fixed at 12 Hz. For the same test conditions, Figures 26 and 27 show the FFT of the transmitted (vertical) bearing forces, left (FLV) and right (FRV). The lines in the graphs are offset an arbitrary value to make more distinctive the influence of rotor speed on the amplitude of rotor response.

In pair with the results shown in Figs. 20 through 23, rotor motion displacements with frequency components at 24 Hz and 70~90 Hz are apparent along the LV direction, as shown in Fig. 24. The system natural frequency is at  $\sim 193$  Hz, nearly invariant with rotor speed. However, the motion amplitudes at the natural frequency increase markedly when the rotor speed increases. Recall that, even without base induced excitation, the rotor starts to whirl at its natural frequency for rotor speeds above 30 krpm and 2.36 bar (ab) pressure into the bearings, see Figs. 12 and 14. For instance, the amplitude component at the natural frequency when the rotor operates at 34 krpm is approximately three times larger than that for operation at 26 krpm, as depicted in Fig. 25. The measurements show the sensitivity of the test rotor-bearing system to excitations of its natural frequency when the bearings are supplied with a low feed pressure.

For the known operating conditions, Appendix D details the predicted rotor motion response amplitudes in time and frequency domains using the Transient Response Analysis feature of XLTRC<sup>2</sup>® [27].

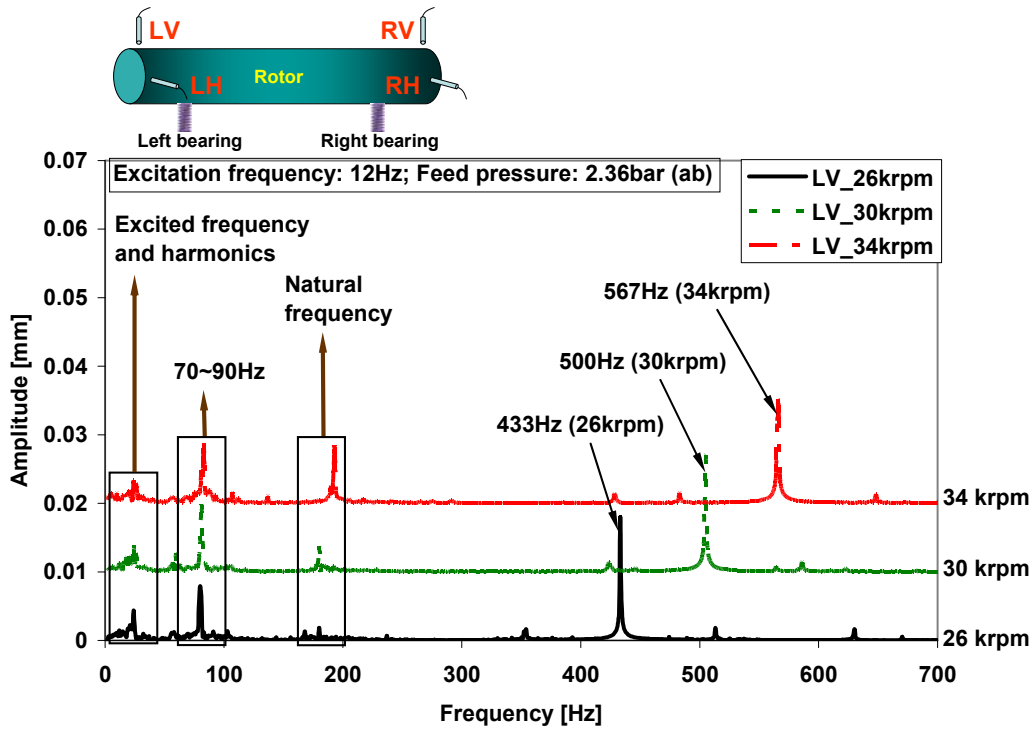


Fig. 24 FFT amplitudes of rotor displacement measured at left end, vertical direction (LV). Rotor speed: 26, 30, and 34 krpm. Bearing feed pressure: 2.36 bar (ab). Shaker induced excitation frequency at 12 Hz.

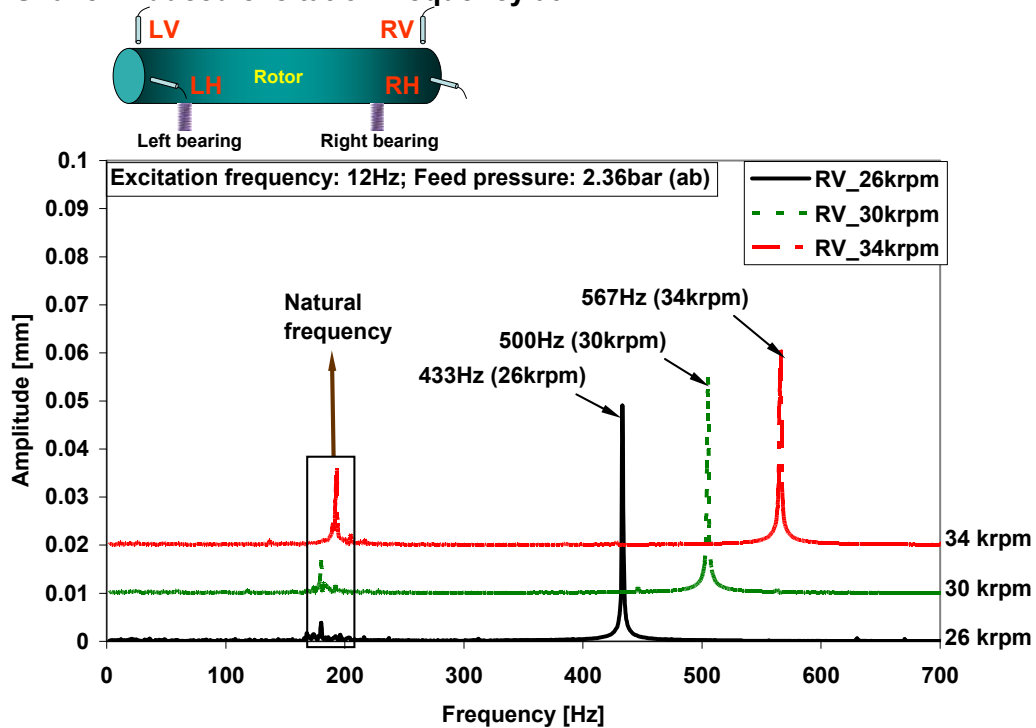


Fig. 25 FFT amplitude of rotor displacement measured at right end, vertical direction (RV). Rotor speed: 26, 30, and 34 krpm. Bearing feed pressure: 2.36 bar (ab). Shaker induced excitation frequency at 12 Hz.

The measured transmitted bearing forces in Figs. 26 and 27 exhibit a similar behavior with those forces depicted in Figs. 22 and 23. The component of bearing force at the system natural frequency increases markedly as rotor speed increases. The results show low amplitude forces, albeit larger than those with synchronous frequency, with frequencies equaling the shaker input excitation frequency of 12 Hz and its harmonics at 24 Hz and 36 Hz.

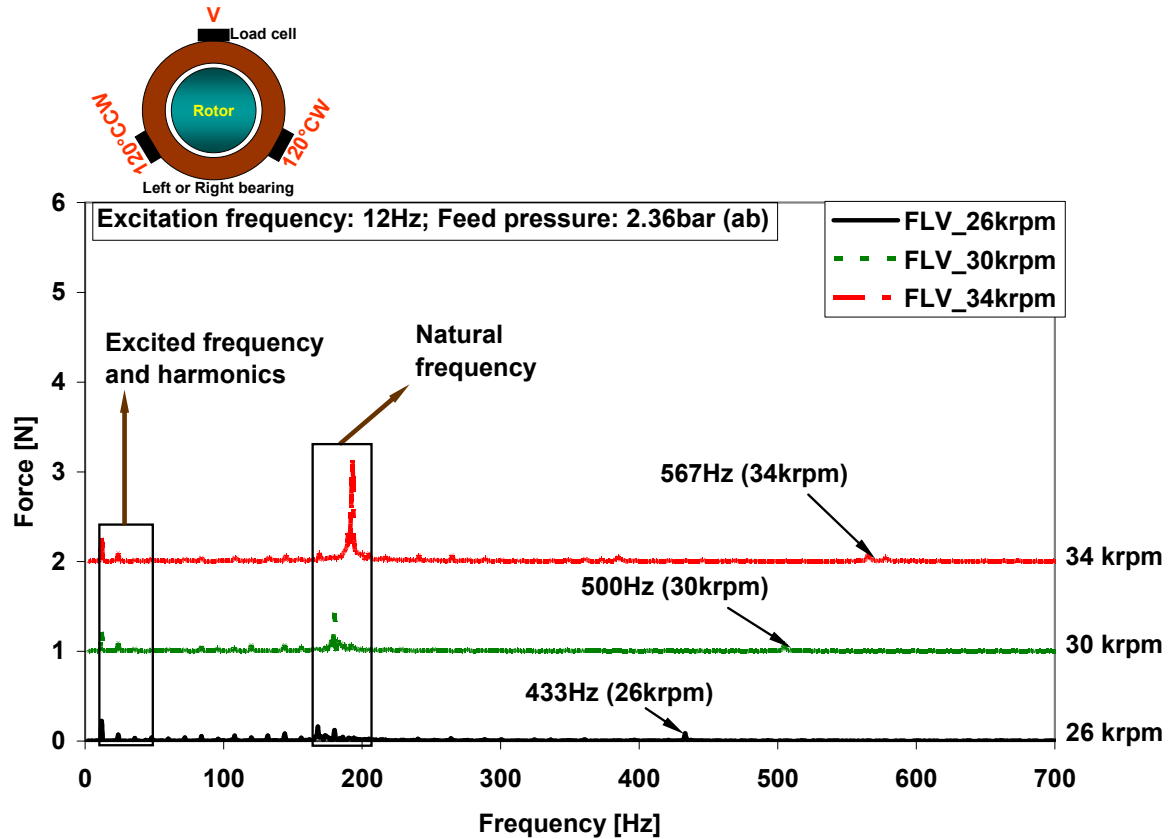
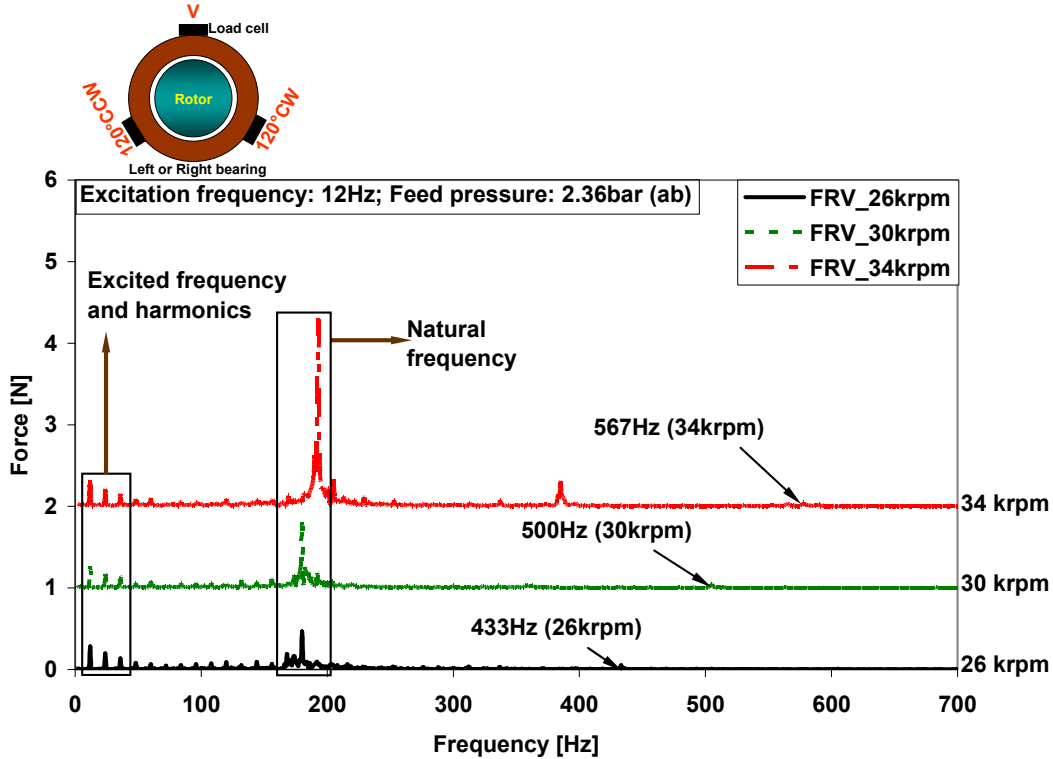


Fig. 26 FFT amplitudes of left bearing force, vertical load cell (FLV). Rotor speed: 26, 30, and 34 krpm. Bearing feed pressure: 2.36 bar (ab). Shaker induced excitation frequency at 12 Hz.



**Fig. 27** FFT amplitudes of right bearing force, vertical load cell (FRV). Rotor speed: 26, 30, and 34 krpm. Bearing feed pressure: 2.36 bar (ab). Shaker induced excitation frequency at 12 Hz.

### Rotor motion response for various shaker excitation frequencies

Figures 28 through 31 depict rotor response amplitudes and bearing forces for measurements with shaker excitation frequency equal to 5, 6, 9 and 12 Hz. Fig. 9 displays the recorded rig base accelerations for the frequencies noted. In the tests, the feed pressure into the bearing is 2.36 bar (ab) and the rotor speed is fixed at 34 krpm.

Recall that 5 Hz is the tilting mode natural frequency of the whole test rig and its two coil springs, see Appendix A. Therefore, with the shaker at 5 Hz, the push load amplitude is smaller than those at other excitation frequencies to guarantee safe operation. At the excitation frequencies of 6, 9, and 12 Hz, the shaker excitation load amplitudes are identical.

As depicted in Figs. 28 and 29, the base induced motions excite the rotor-bearing system natural frequency, ~193 Hz. The amplitudes of motion at this frequency increase with the shaker excitation frequency. For reference, the figures include data recorded without any base excitation.

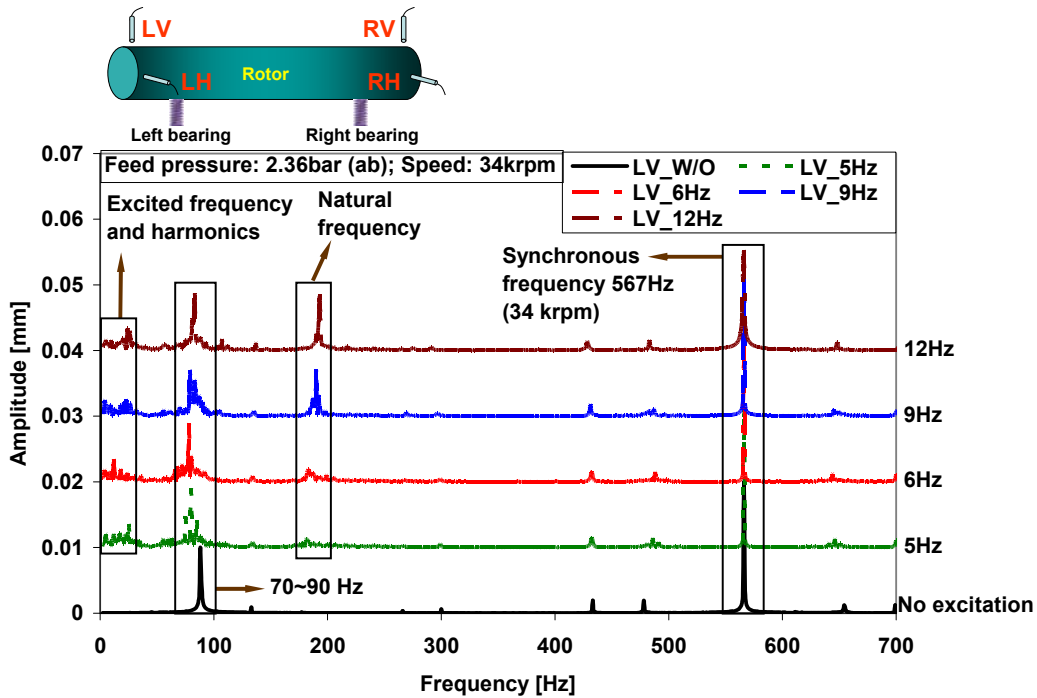


Fig. 28 FFT amplitudes of rotor displacement measured at left end, vertical direction (LV). Shaker induced excitation frequency at 5Hz, 6Hz, 9Hz and 12Hz. Rotor speed: 34 krpm. Bearing feed pressure: 2.36 bar (ab).

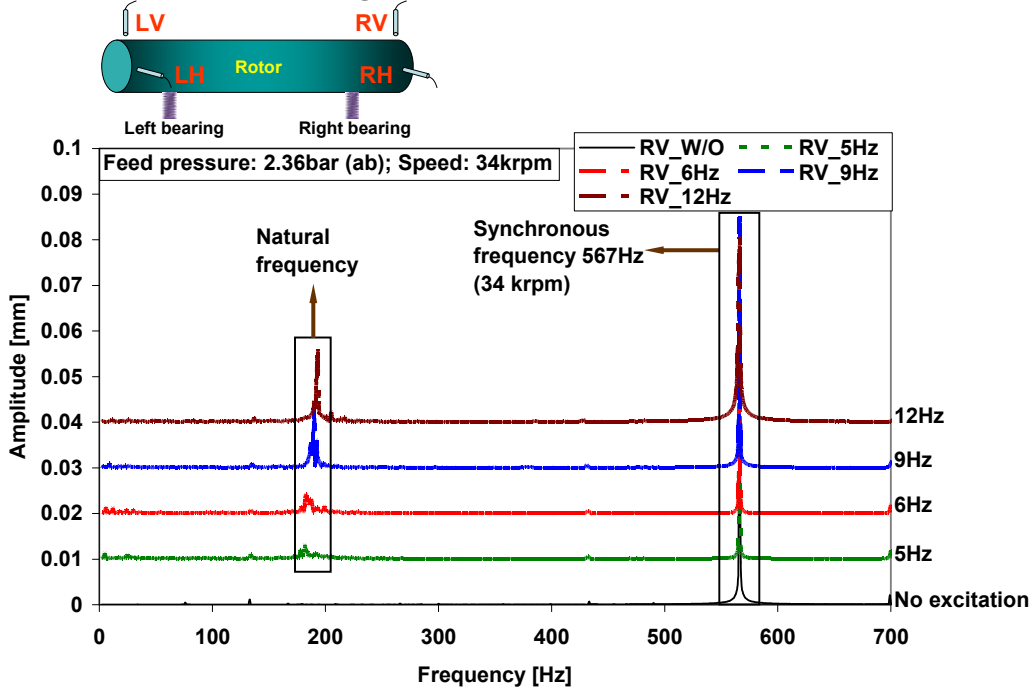
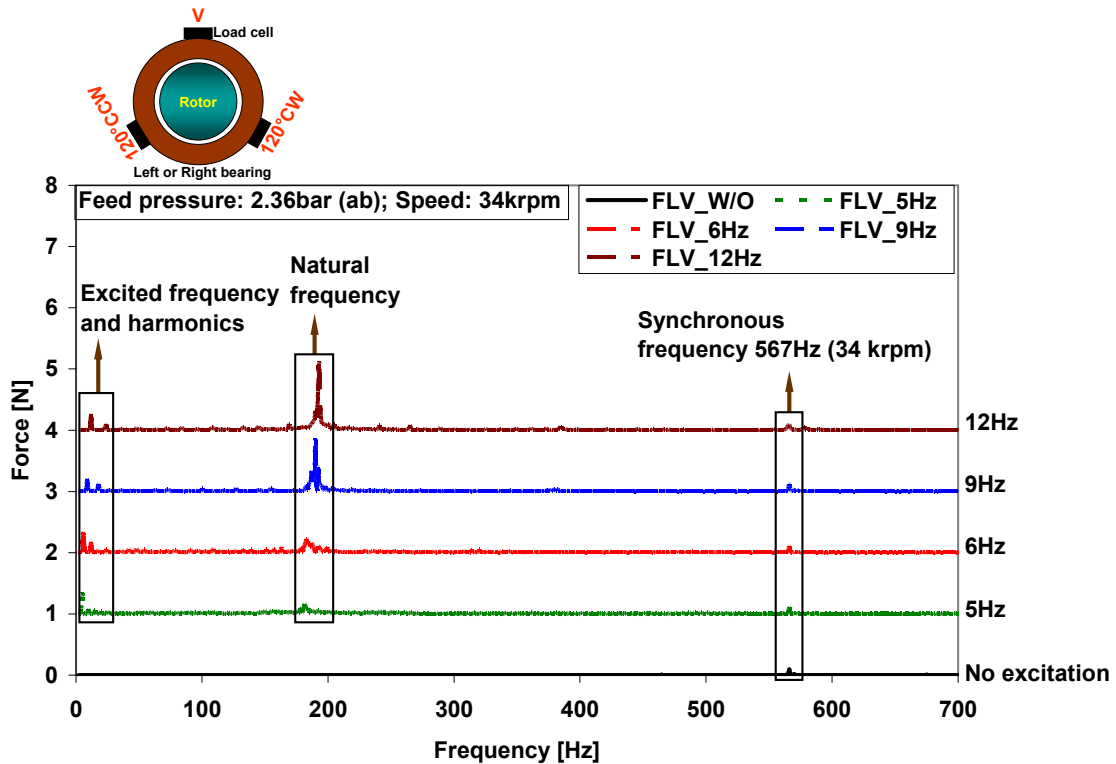


Fig. 29 FFT amplitudes of rotor displacement measured at right end, vertical direction (RV). Shaker induced excitation frequency at 5Hz, 6Hz, 9Hz and 12Hz. Rotor speed: 34 krpm. Bearing feed pressure: 2.36 bar (ab).



In the bearing forces shown in Figs. 30 and 31, the base motion brings significant load amplitudes at the system natural frequency. These amplitudes become larger with a higher excitation frequency. Incidentally, note that the components of load at the synchronous frequency are insignificant, thus denoting the good isolation of the rotor-bearing system.



**Fig. 30** FFT amplitudes of left bearing load, from vertical load cell (FLV). Shaker induced excitation frequency at 5Hz, 6Hz, 9Hz and 12HZ. Rotor speed: 34 krpm. Bearing feed pressure: 2.36 bar (ab).

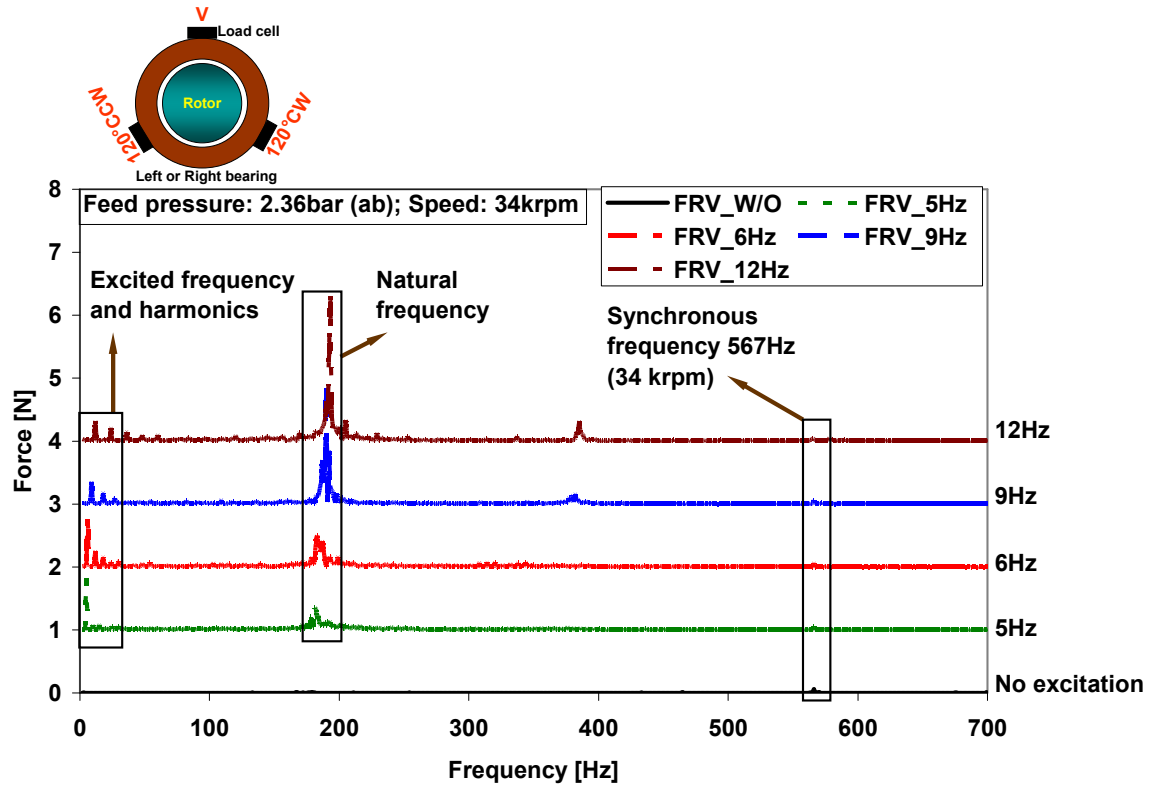


Fig. 31 FFT amplitudes of right bearing load, from vertical load cell (FRV). Shaker induced excitation frequency at 5Hz, 6Hz, 9Hz and 12Hz. Rotor speed: 34 krpm. Bearing feed pressure: 2.36 bar (ab).

## Conclusions

Oil-free microturbomachinery (MTM) utilizing gas bearings are often subjected to base or foundation transferred load excitations: passenger and commercial transportation vehicles experiencing intermittent base excitations from road conditions, and (multiple) periodic load excitations from internal combustion (IC) engines in turbochargers, for example. The base excitations can produce permanent damage, even failure, due to hard collision or rubbing contact between a rotor and its bearings. Hence, it is essential to evaluate the reliability of rotor-air bearing systems to withstanding base load excitations.

In the present investigation, an electromagnetic shaker delivers periodic load excitations to the base plate supporting a rotor-bearing test rig. The whole rotor-bearing system is supported on two soft coil springs (whole test rig natural frequency of  $\sim 5$  Hz). The 0.825 kg rotor is supported on two flexure pivot tilting pad hydrostatic gas bearings (FPTPBs). The shaker induced base load excitations simulate practical external excitations, such as uneven road surfaces or IC engine induced vibrations in turbochargers, for example. In most practical cases, the base motion frequencies are low respective to the operating rotational speed of the rotor-bearing system.

With shaker induced excitations at 5, 6, 9, and 12 Hz, four types of tests are conducted. The first tests are rotor speed coast down measurements (from 35 krpm) with the gas bearings supplied with 2.36, 3.72, and 5.08 bar (ab) feed pressures. The second tests are at a fixed rotor speed and the bearings supply pressure is increased from 2.36 bar to 5.08 bar (ab). In the third tests, the feed pressure into the gas bearings is fixed and the rotor speed increases step-wise (26, 30, and 34 krpm). Finally, the shaker input excitation frequency increases (5, 6, 9, and 12 Hz), while the feed pressure into the gas bearings and the rotor speed are fixed at 2.36 bar (ab) and 34 krpm, respectively.

It is important to note that, since the shaker push rod is not affixed into the test rig base plate, the excitation system consists of a number of intermittent impacts over prescribed time intervals. The shaker induced base acceleration has a peak amplitude of 1.7 g with frequency components at the main input excitation frequency (from shaker) and its harmonics. The peak acceleration is  $\sim 0.2$  g in the frequency domain.

Rotor speed coast down tests, without the shaker acting, evidence the system natural frequency for the gas bearings supplied at increasing feed pressures. These frequencies

are 193 Hz at 2.36 bar (ab) and increasing to 243 Hz at 5.08 bar (ab) supply pressure. The amplitudes of synchronous rotor response is not affected by the base excitations, since the shaker induced frequencies (5-12 Hz) are quite low with respect to the operating speed of the test rig, typically above 3 krpm (50 Hz). Due to the unconstrained connection of the shaker push rod to the test rig base plate, the base motions are not single frequency, but contain multiple super harmonics of the main shaker frequency. Hence, the rotor motion response (relative to the rig base) also shows super harmonics of base excitation, in particular the second harmonic, and most importantly, the rotor-bearing system natural frequency. The amplitudes of motion at the natural frequency are small with respect to those synchronous with rotor speed. The excitation of the rotor-bearing system natural frequency does not mean the system exhibits rotordynamic instability.

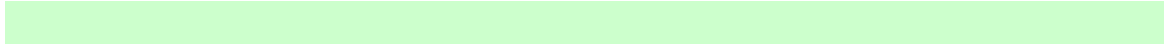
While the shaker exciting the test rig at increasing frequencies (5-12 Hz), the tests aim to quantify the effect of gas bearing feed pressure and rotor operating speed on the rotordynamic displacements and bearing reaction forces. At the left rotor end, vertical direction, the recorded rotor motions show (subsynchronous) frequency components at the shaker main excitation frequency and its harmonics and the rotor-bearing system natural frequency. At the right rotor end, vertical direction, rotor motions show only the natural frequency. In general, the rotor amplitude of motion at the system natural frequency increases in amplitude as the gas bearing feed pressure decreases, as the rotor operating speed increases, or as the shaker input excitation frequency increases (5~12 Hz). Thus, the test rotor-bearing system is highly sensitivity to the base motions that excite its natural frequency when the rotor runs at a high speed or when the gas bearings are fed with a low pressure.

Measured bearing reaction forces show dominance of load components at the rotor-bearing system natural frequency (193 Hz to 243 Hz) rather than at the (high) frequency synchronous with rotor speed. This is so since the test rotor typical operating speed (>25 krpm) is well above its natural frequency. Hence, the rotor-bearing demonstrates reliable isolation.

Transient response analysis predictions from XLTRC<sup>2</sup>®[27] and analytical predictions from a simple rigid rotor model give results that are in agreement with the measured rotor motions (relative to the base or foundation), see Appendices D and E. In

the analyses, the measured base acceleration is split, using Fourier analysis, into frequency components.

The experimental results demonstrate the reliability of the test rig to undergoing periodic base load excitations. The verified robustness of the rotor-hybrid gas bearing system to withstanding both periodical and transient base excitations effectively promotes the applications of FPTPBs in oil-free microturbomachinery.



## References

- [1] San Andrés, L., and Ryu, K., 2006, “Test Results for Load-On-Pad and Load-Between-Pad Hybrid Flexure Pivot Tilting Pad Gas Bearings,” TL-B&C-1-06, Research Progress Report to the Turbomachinery Laboratory, Texas A&M University, College Station, TX.
- [2] Fuller, D. D., 1969, “A Review of the State-of-the-Art for Design of Self-Acting Gas-Lubricated Bearing,” *ASME J. Lubr. Technol.*, **91**, pp. 1-16.
- [3] Armentrout, R. W., and Paquette, D. J., 1993, “Rotordynamic Characteristics of Flexure-Pivot Tilting-Pad Journal Bearings,” *STLE Tribol. Trans.*, **36**, pp. 443-451.
- [4] Zhu, X., and San Andrés, L., 2007, “Rotordynamic Performance of Flexure Pivot Hydrostatic Gas Bearings for Oil-Free Turbomachinery,” *ASME J. Eng. Gas Turbines Power*, **129**, pp. 1020-1027.
- [5] San Andrés, L., 2006, “Hybrid Flexure-Pivot Tilting-Pad Gas Bearings: Analysis and Experimental Validation,” *ASME J. Tribol.*, **128**, pp. 551-558.
- [6] San Andrés, L., and Ryu, K., 2008, “Flexure Pivot Tilting Pad Hybrid Gas Bearings: Operation with Worn Clearances and Two Load-Pad Configurations,” *ASME J. Eng. Gas Turbines Power*, **130**, 042506.
- [7] San Andrés, L., and Ryu, K., 2008, “Hybrid Gas Bearings with Controlled Supply Pressure to Eliminate Rotor Vibrations while Crossing System Critical Speeds,” *ASME J. Eng. Gas Turbines Power*, **130**, 062505.
- [8] Ryu, K., and San Andrés, L., 2008, “Dynamic Forced Response of a Rotor-Hybrid Gas Bearing System due to Intermittent Shocks,” TRC-B&C-1-08, Research Progress Report to the Turbomachinery Research Consortium, Texas A&M University, College Station, TX.
- [9] Srinivasan, V., and Soni, A. H., 1982, “Seismic Analysis of Rotating Mechanical Systems—A Review,” *Shock Vib. Dig.*, **14**, pp. 13-19.
- [10] Samali, B., Kim, K. B., and Yang, J. N., 1986, “Random Vibration of Rotating Machines under Earthquake Excitations,” *ASCE J. Eng. Mech.*, **112**, pp. 550-565.
- [11] Kim, K. B., Yang, J. N., and Lin, Y. K., 1986, “Stochastic Response of Flexible Rotor-Bearing Systems to Seismic Excitations,” *Prob. Eng. Mech.*, **1**, pp. 122-130.
- [12] Kameswara Rao, C., and Mirza, S., 1989, “Seismic Analysis of High-Speed Rotating Machinery,” *Nucl. Eng. Des.*, **111**, pp. 395-402.
- [13] Gaganis, B. J., Zisimopoulos, A. K., Nikolakopoulos, P. G., Papadopoulos, C. A., 1999, “Modal Analysis of Rotor on Piecewise Linear Journal Bearings Under Seismic Excitation,” *ASME J. Vib. Acoust.*, **121**, pp. 190–196.
- [14] Suarez, L. E., Singh, M. P., Rohanimanesh, M.S., 1992, “Seismic Response of Rotating Machines,” *Earthquake Eng. Struct. Dyn.*, **21**, pp. 21–36.
- [15] Tessarzik, J. M., Chiang, T., and Badgley, R. H., 1974, “The Response of Rotating Machinery to External Random Vibration,” *ASME J. Eng. Indus.*, **96**, pp. 477-489.
- [16] Duchemin, M., Berlioz, A., Ferraris, G., 2006, “Dynamic Behavior and Stability of a Rotor Under Base Excitation,” *ASME J. Vib. Acous.*, **128**, pp. 576-585.

- [17] Driot, N., Lamarque, C. H., and Berlioz, A., 2006, "Theoretical and Experimental Analysis of a Base-Excited Rotor," *ASME J. Comput. Nonlinear Dyn.*, **1**, pp. 257-263.
- [18] Subbiah, R., Bhat, R. B., and Sanker, T. S., 1985, "Response of Rotors Subjected to Random Support Excitations," *ASME J. Vib. Acoust. Stress Reliab. Design*, **107**, pp. 453-459.
- [19] Maruyama, A., 2007, "Prediction of Automotive Turbocharger Nonlinear Dynamic Forced Response with Engine-Induced Housing Excitations: Comparisons to Test Data," Masters Thesis, Texas A&M University, College Station, TX.
- [20] Walton, J. F., Heshmat, H., and Tomaszewsky, M. J., 2008, "Testing of a Small Turbocharger/Turbojet Sized Simulator Rotor Supported on Foil Bearings," *ASME J. Eng. Gas Turbines Power*, **131**, 035001.
- [21] Heshmat, H., and Walton, J. F., 2000, "Oil-Free Turbocharger Demonstration Paves Way to Gas Turbine Engine Applications," ASME paper 2000-GT-620.
- [22] Lee, A. S., Kim, B. O., and Kim, Y. C., 2006, "A Finite Element Transient Response Analysis Method of a Rotor-Bearing System to Base Shock Excitation Using the State-Space Newmark Scheme and Comparisons with Experiments," *J. Sound Vib.*, **297**, pp. 595-615.
- [23] Lee, A. S., and Kim, B. O., 2007, "A FE Transient Response Analysis Model of a Flexible Rotor-Bearing System with Mount System to Base Shock Excitation," ASME paper GT2007-27677.
- [24] Jayson, E. M., Murphy, J., Smith, P. W., and Talke, F. E., 2003, "Effects of Air Bearing Stiffness on a Hard Disk Drive Subject to Shock and Vibration," *ASME J. Tribol.*, **125**, pp. 343-349.
- [25] Jayson, E. M., and Talke, F. E., 2005, "Optimization of Air Bearing Contours for Shock Performance of a Hard Disk Drive," *ASME J. Tribol.*, **127**, pp. 878-883.
- [26] Vance, J. M., 1988, *Rotordynamics of Turbomachinery*, Wiley, New York.
- [27] XLTRC<sup>2</sup>® Rotordynamics Software Suite v. 2.1, 2002, Turbomachinery Laboratory, Texas A&M University, College Station, TX.
- [28] De Santiago, O. C., and San Andrés, L., 2007, "Field Methods for Identification of Bearing Support Parameters— Part II: Identification from Rotor Dynamic Response due to Imbalances," *ASME J. Eng. Gas Turbines Power*, **129**, pp. 213-219.

## Appendix A. Measurement of test rig natural frequency

Impact load tests are conducted to measure the whole test rig natural frequency. The test procedure follows that in Ref. [8]. A hammer with hard steel tip delivers impact loads to the test rig base plate. An accelerometer, sensitivity of 5mV/g, measures the accelerations induced by external impact forces. The accelerometer is located at six positions: test rig base plate, top of motor casing, top of left bearing housing, top of right bearing housing, top of left end casing, and top of right end casing, see Figure A.1. Figure A.2 shows the measured accelerations on the four positions with distinctive peaks at 5 Hz, i.e. the tilting-mode natural frequency of the whole test rig on the soft coil springs. Note the sharp peak acceleration response is indicative of little damping. The measured acceleration at base plate is around 0.27 g, while the accelerations at motor casing, left bearing housing, and right bearing housing are much smaller, around 0.15 g. In addition, Figures A.3 and A.4 show similar measured accelerations (5 Hz) at motor casing and left or right end casings. That is, the whole test rig, including the main steel cylindrical body, bearing housings, and end casings, behaves as a rigid body when base load excitations are introduced.

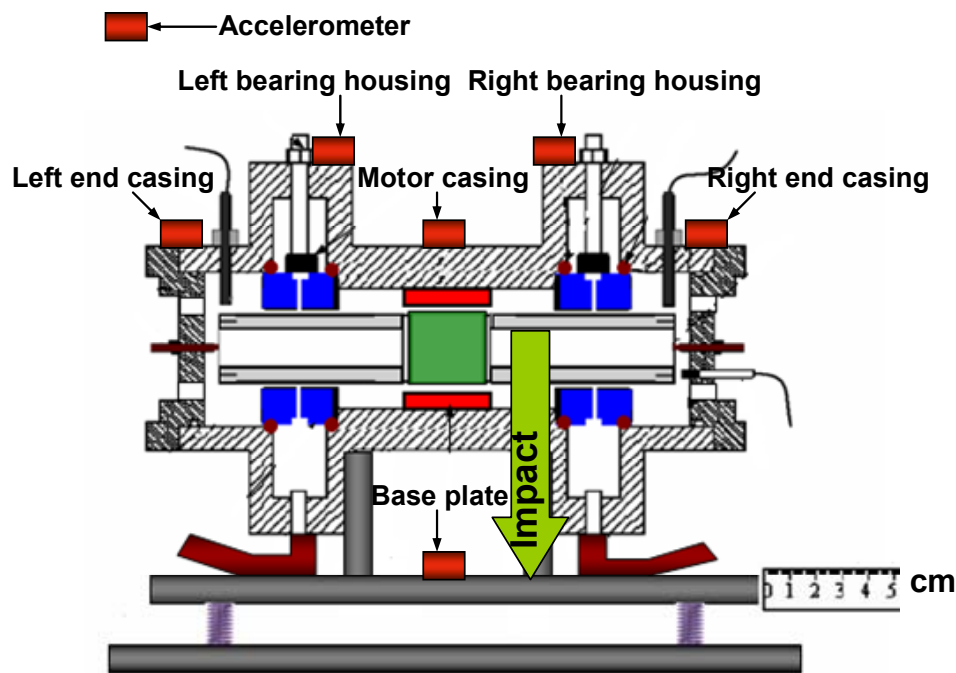


**Fig. A.1 Schematic view of test rig and acceleration measurement positions for impact hammer measurements**



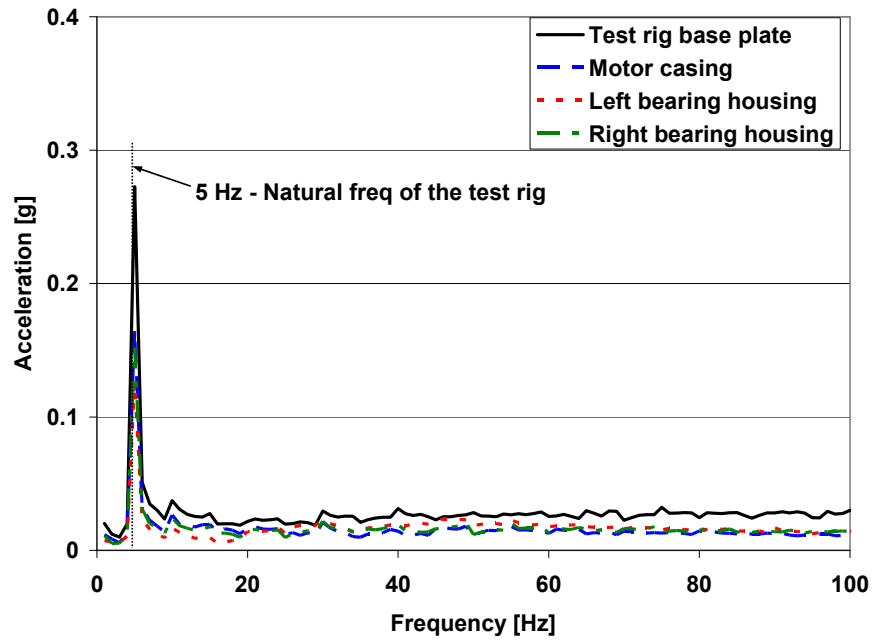


Fig. A.2 Accelerations recorded at test rig base plate, motor casing, left bearing housing, and right bearing housing. From impact loads on base plate.

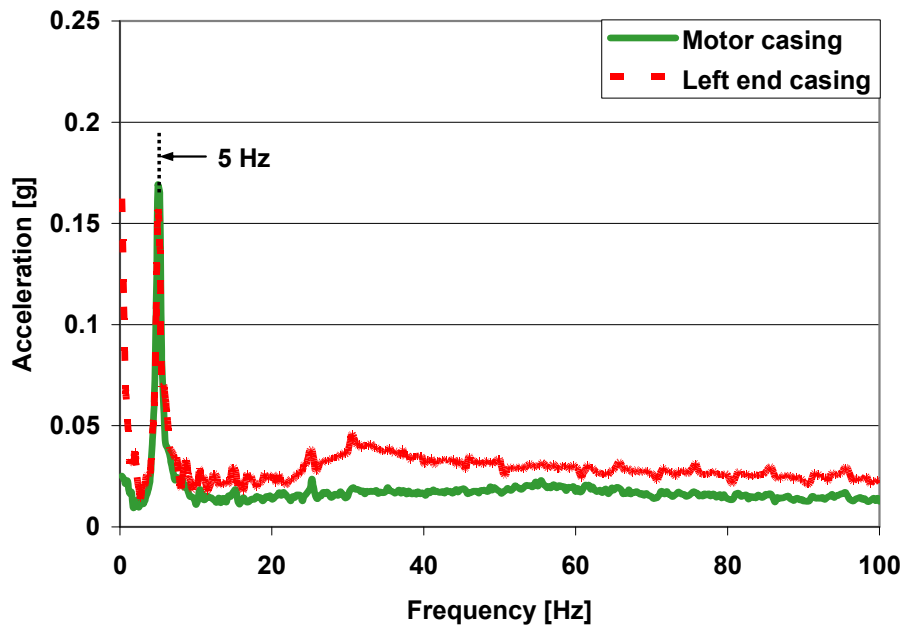


Fig. A.3 Accelerations recorded at motor casing and left end casing. From impact loads on base plate.

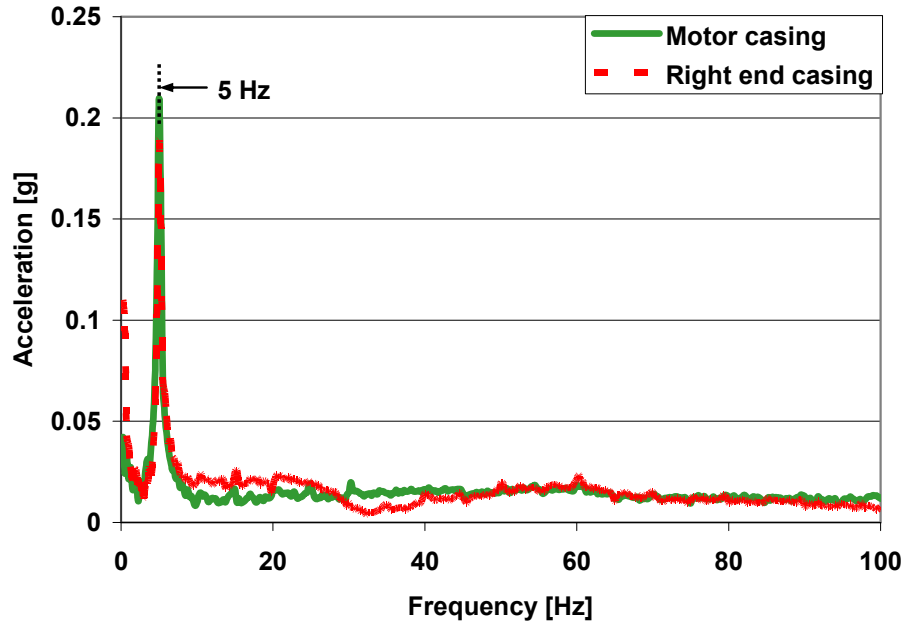
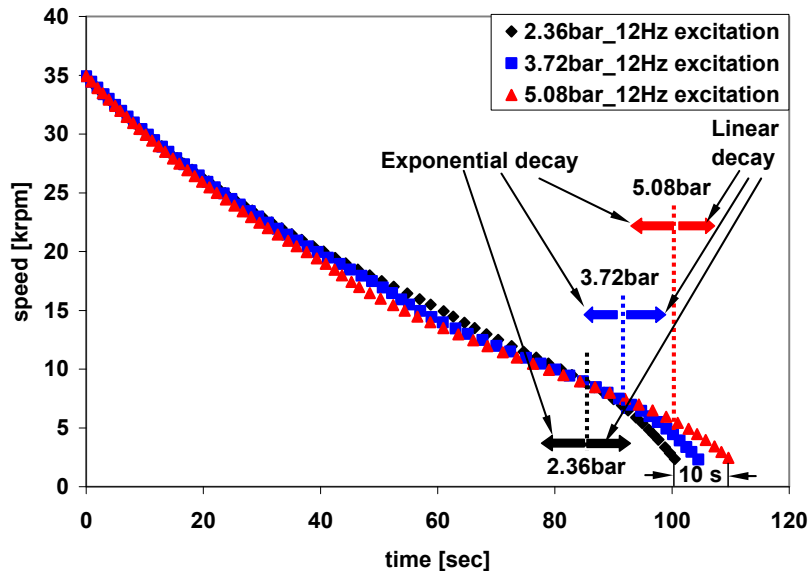


Fig. A.4 Accelerations recorded at motor casing and right end casing. From impact loads on base plate.

## Appendix B. Measurements of rotor coast down speed versus time

In tests with shaker induced base motions with frequency of 12 Hz, Figure B.1 depicts the rotor coast down speed versus time. The curves show measurements with increasing feed pressures into the gas bearings. The speed coast down time increases slightly (10 sec difference) as the bearing feed pressure is raised. From mechanical systems modeling, an exponential decay denotes viscous friction, whereas a linear decay corresponds to dry friction, i.e., rubbing between the rotor and its bearings.

For a supply pressure equal to 5.08 bar (ab), dry friction only appears below 6 krpm. However, at a bearing feed pressure of 2.36 bar (ab), rubbing occurs below 9 krpm. Therefore, as expected, increasing the gas supply pressure into the bearings is an effective approach to reduce rotor rubbing at speed coast down operating conditions, i.e. a delay in the touchdown speed.



**Fig. B.1 Measured rotor coast down speed versus time. Shaker induced excitation frequency: 12 Hz. Bearing feed pressures: 2.36, 3.72, and 5.08 bar (ab).**

Figure B.2 shows the rotor coast down speed versus time for operation with the gas bearings supplied with feed pressure of 2.36 bar (ab). The coast down test is conducted three times to verify repeatability of the measurements. The curves denote measurements for shaker excitation frequency equaling 6, 9, and 12 Hz. Without (shaker induced) base motions, the rotor coast down time is around 110 sec, longer than the coast down time

with the shaker induced excitations. At a shaker excitation frequency of 6 Hz, the coast down time is less than 100 sec, with rubbing occurring below 10 krpm. Note that the excitation frequency of 6 Hz is just above the natural frequency ( $\sim 5$  Hz) of the whole test rig supported on its two coil springs.

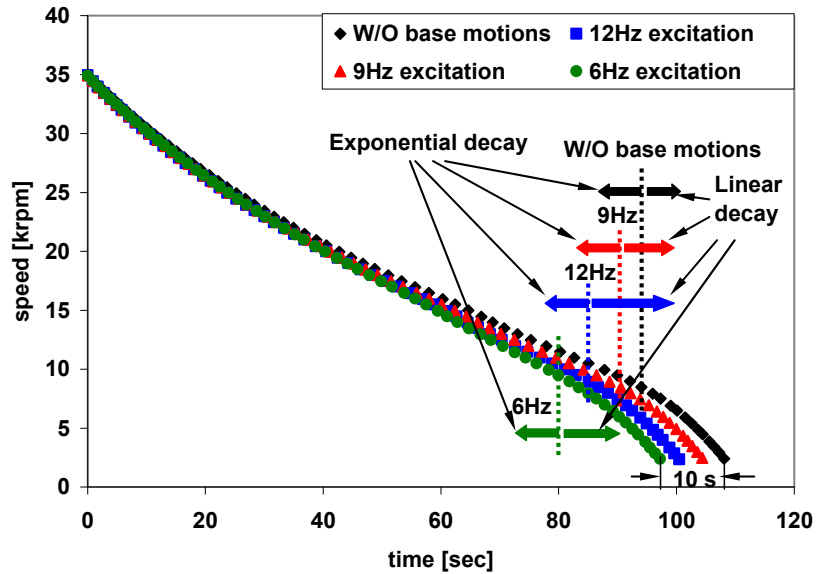


**Fig. B.2 Measured rotor coast down speed versus time. Shaker induced excitation frequencies: 6, 9, and 12 Hz. Bearing feed pressure: 2.36 bar (ab).**

## Appendix C. Predicted stiffness and damping force coefficients for gas bearings

The prediction of bearing force coefficients is derived from the model developed in Ref. [5]. Figure C.1 shows the coordinate system for bearing analysis. Recall that the test rig base is tilted statically  $10^\circ$  around its hinged fixture (see Figure 1). Note the load configuration is close to a load-on-pad (LOP) condition.

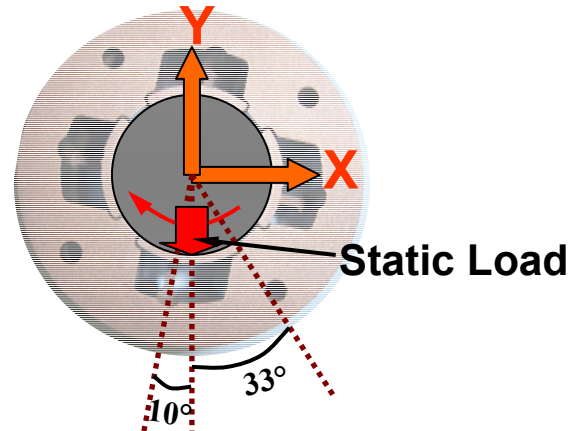


**Fig. C.1 Schematic view of coordinate system for bearing analysis. Test rig (and bearing) tilted  $10^\circ$  around hinged fixture.**

Figures C.2 and C.3 depict the predicted rotor eccentricities and attitude angles for the left bearing. The static load on this bearing is 4.045 N, i.e., half the rotor weight. External pressurization into the bearings leads to small eccentricities, which further decrease as the operating speed increases. The variation in eccentricity indicates that the bearing direct stiffness coefficients increase with both pressurization magnitude and rotor speed. The journal attitude angle decreases with pressurization but increases with rotor speed, indicating that cross-coupled stiffnesses decrease with increases in feed pressure, but increase with rotor speed.

Figures C.4 and C.5 present the bearing direct and cross-coupled stiffnesses and damping coefficients, respectively. These coefficients are synchronous, i.e. evaluated at a frequency coinciding with the rotor angular speed. The supply pressure acts to increase the direct stiffness coefficients, while decreasing the direct damping coefficients. The direct stiffness coefficients increase with rotor speed, but the direct damping coefficients show no marked correlation with rotor speed. Note that the static load is small and the rotor eccentricity is also small, hence the bearing shows  $K_{xx} \approx K_{yy}$  and  $K_{xy} \approx -K_{yx}$ , in

particular for the highest supply pressures, 3.72 bar and 5.08 bar (ab). Both the cross-coupled stiffness and damping coefficients increase with rotor speed, while decreasing with the magnitude of supply pressure.

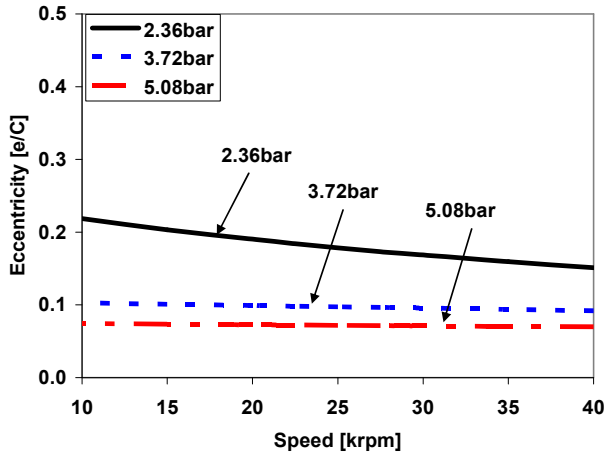


Fig. C.2 Predicted static journal eccentricity ( $e/C$ ) for increasing feed pressures into (left) gas bearing.

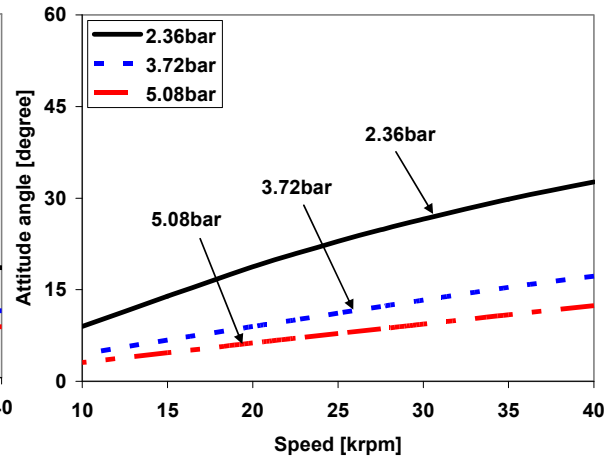


Fig. C.3 Predicted attitude angle for increasing feed pressures into (left) gas bearing.

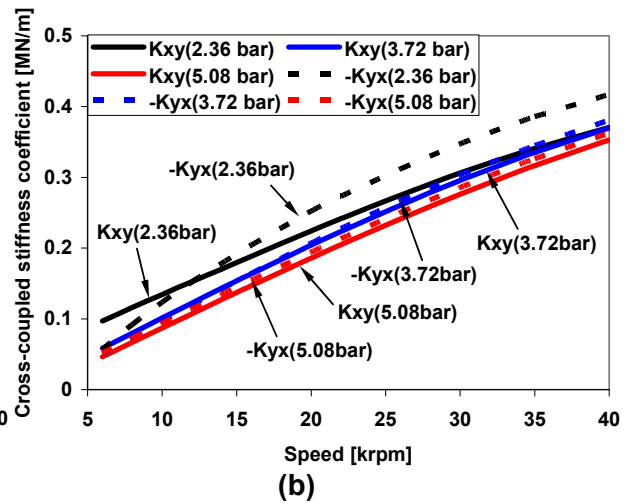
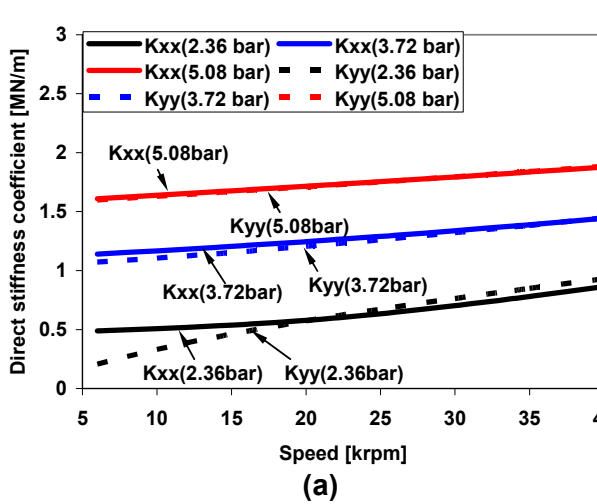
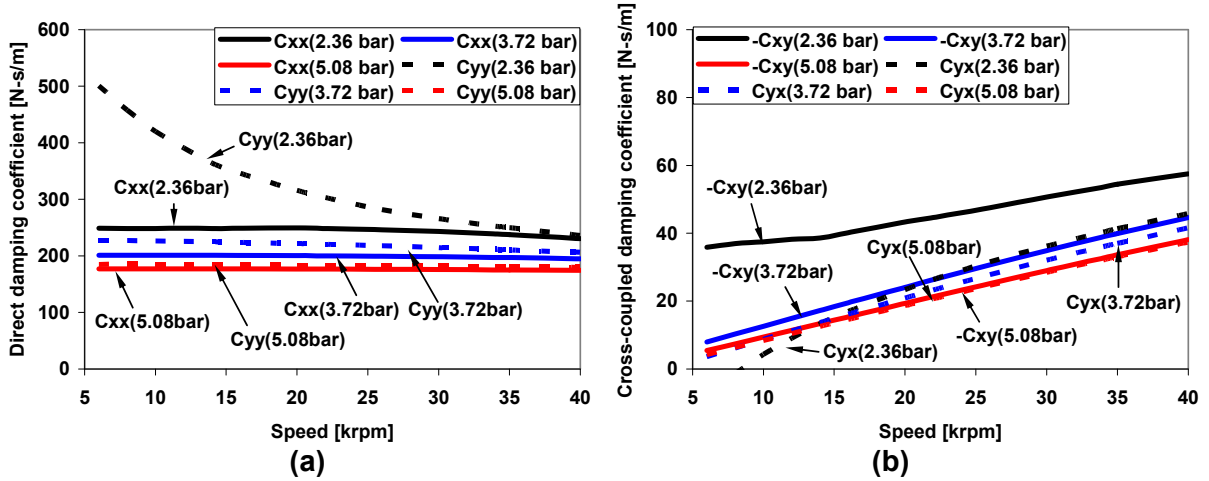


Fig. C.4 Stiffness coefficients of gas bearing versus rotor speed. Predictions for increasing supply pressures into bearing. (a) direct and (b) cross-coupled stiffnesses (synchronous speed) coefficients.



**Fig. C.5 Damping coefficients of gas bearing versus rotor speed. Predictions for increasing supply pressures into bearing. (a) direct and (b) cross-coupled damping (synchronous speed) coefficients.**

## Appendix D. XLTRC<sup>2</sup>® predicted (absolute) rotor motion response due to base excitation

The prediction of rotor response is performed using the Transient Response Analysis capability of XLTRC<sup>2</sup>®. The finite element structural model of the rotor includes 22 elements, as shown in Figure D.1. Bearing supports, represented by stiffness and damping coefficients, connect the rotor to its base or ground, which is subjected to periodic excitations. For the predictions, the bearing feed pressure is fixed at 2.36 bar (ab). Synchronous speed force coefficients are used in the rotordynamic transient response analysis<sup>1</sup>.

At rotor speeds equaling 26, 30, and 34 krpm, Table D.1 lists the predicted natural frequencies corresponding to the conical and cylindrical (rigid body) modes. The natural frequency increases slightly with rotor speed. Figure D.2 depicts the mode shapes when the rotor operates at 34 krpm. Within the speed range of the tests, the rotor can be regarded as nearly rigid.

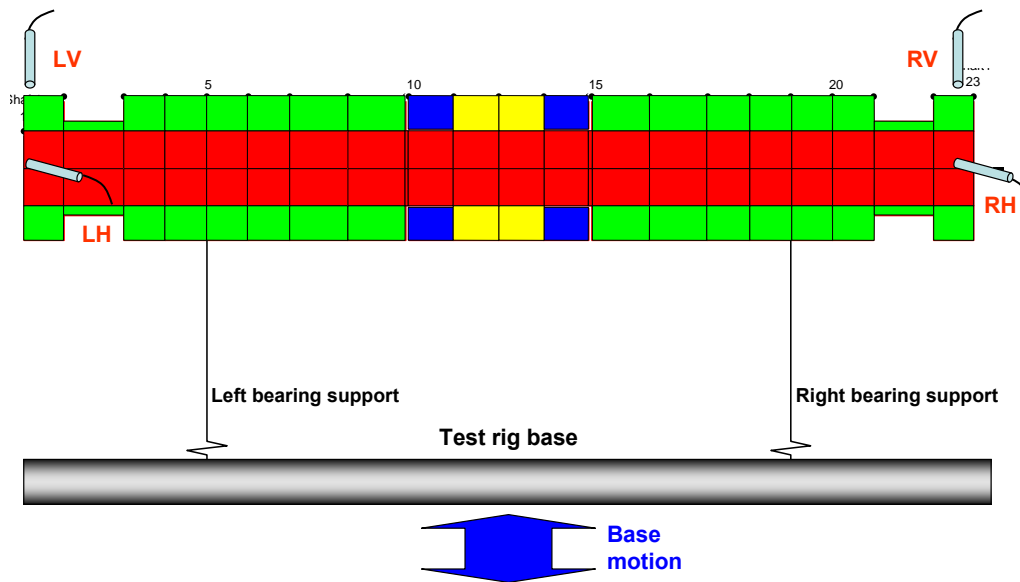


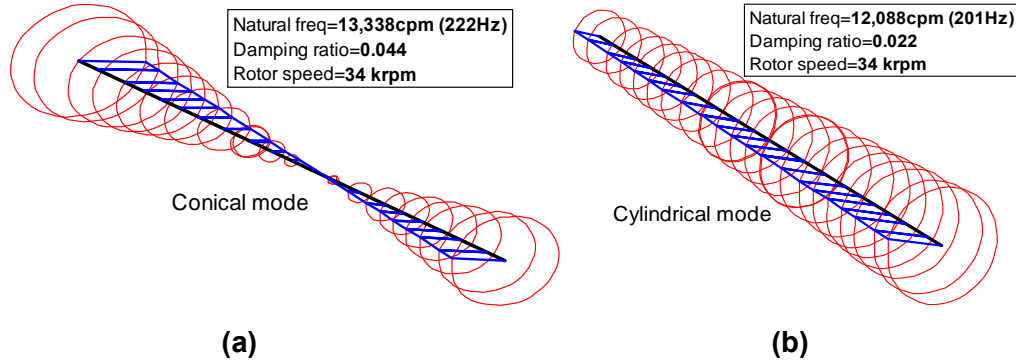
Fig. D.1 FE structural model of rotor and location of bearing supports

Table D.1 Predicted rotor-bearing system natural frequency at three rotor speeds. Gas bearing supply pressure=2.36 bar (ab).

	26 krpm	30 krpm	34 krpm
Conical	202 Hz	212 Hz	222 Hz
Cylindrical	185 Hz	193 Hz	201 Hz

<sup>1</sup> This is a limitation of the software used. Gas bearings, as many other fluid film bearing elements, have frequency dependent force coefficients.





**Fig. D.2 Predicted rotor mode shapes. Forward whirling. Rotor speed: 34 krpm. (a) Conical mode; (b) Cylindrical mode.**

Table D.2 lists the measured (cylindrical mode) natural frequency at three rotor speeds, see Figs. 24 and 25 for the FFTs of rotor motion with bearings supplied at 2,36 bar. At the respective rotor speed, the recorded rotor-bearing natural frequency, excited by the base motion, is close to the predicted natural frequency. The comparison reveals a difference of at most 10 Hz. Note that in actuality, the bearing force coefficients are frequency dependent. However, only synchronous speed bearing force coefficients are used in the predictions. Hence an argument explains the differences.

**Table D.2 Measured natural frequency at three rotor speeds. Gas bearing supply pressure=2.36 bar (ab).**

Rotor speed	26 krpm	30 krpm	34 krpm
<b>Natural Frequency</b>	180 Hz	180 Hz	193 Hz
<b>Predicted Cylindrical</b>	185 Hz	193 Hz	201 Hz

In XLTRC<sup>2</sup>®, the base excitation is input at the bearing stations as a collection of single frequency acceleration amplitudes and phase, as in the components of a Fourier series. Presently, the recorded base acceleration is split, using Fourier analysis, into frequency components at 12, 24, 36, 48, 60 Hz, and the respective rotor-bearing natural frequency. Figure D.3 shows the amplitude of acceleration and its associated frequencies

for input base acceleration. The input base acceleration at 12 Hz and its harmonics simulate the measured shaker induced base acceleration, as depicted in Fig. 9 (d). Note that 201 and 222 Hz are the predicted system natural frequencies at the speed of 34 krpm, see Table D.1. In XLTRC<sup>2</sup>®, the input base acceleration is along the vertical direction, while the horizontal direction component is of insignificant magnitude. Recall that the test rig base plate is tilted statically  $\sim 10^\circ$  from the horizontal plane.

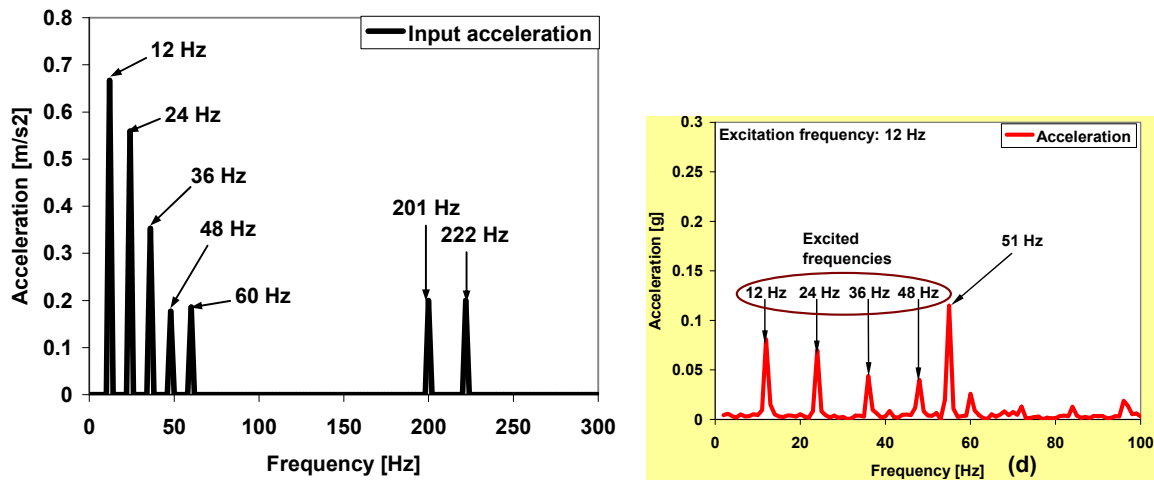


**Fig. D.3 Components of base excitation acceleration for prediction of rotor response. Rotor speed: 34 krpm. Main frequency 12 Hz. (Inset Figure 9(d): measured acceleration).**

Imbalance masses used in XLTRC<sup>2</sup>® are:  $m_1 = 0.1$  g,  $m_2 = 0.6$  g,  $\Phi_1 = 0^\circ$ , and  $\Phi_2 = 0^\circ$ .  $m_1$  and  $m_2$  are the estimated remnant imbalance masses attached at radii  $r_1$  and  $r_2$  at angular locations  $\Phi_1$  and  $\Phi_2$  in the rotor end planes.  $r_1 = r_2 = 12$  mm. Subscripts 1 and 2 denote left and right rotor end planes, respectively.

The time span for numerical integration of the rotor-bearing equations of motion is 0.8 sec, and the frequency spectrum is up to 1 kHz. The time step is only 0.2 ms to ensure accuracy. The initial condition is the steady state rotor response after transient excitation. The numerical model integrator is a Gear (STIFF) method.

For rotor speeds equal to 26, 30 and 34 krpm, figures D.4, D.5 and D.6 depict the predicted and measured rotor motion response at the rotor left end, vertical direction (LV). Note that the XLTRC<sup>2</sup>® predicted rotor response refers to a fixed coordinate system (absolute displacement), while the measured rotor displacement is, in actuality, relative to the test rig (bearing housings).

In the figures, a logarithmic scale for the amplitude of displacements is selected for illustrative purposes. The predicted rotor motion exhibits components at 12 Hz and its harmonics, the rotor-bearing system natural frequencies, and the synchronous frequency. The predicted and measured rotor motion components with synchronous frequency are in good agreement. As with the measured motion with components at the natural frequency, the predicted amplitude of motion at the system natural frequency increases in magnitude as the rotor speed increases, indicating lesser damping (see Fig. C.5). Note that the measured rotor motion amplitudes at the natural frequency (180 Hz) are somewhat larger than the predicted ones at 185 Hz and 202 Hz. The difference is due to the dissimilar bearing force coefficients, actual and predicted. In addition, the measured rotor motion response has motion components with frequencies ranging from 70 to 90 Hz. These frequencies are apparent even without base motions, see Fig. 28. Their source is unknown. The predicted rotor motion amplitudes at 12 Hz and its super harmonics are slightly larger than the measured ones, in particular at the main input frequency (12 Hz). Recall that the predicted response is relative to an absolute (stationary) coordinate system rather than the relative to the bearing housings, as in the measurements.

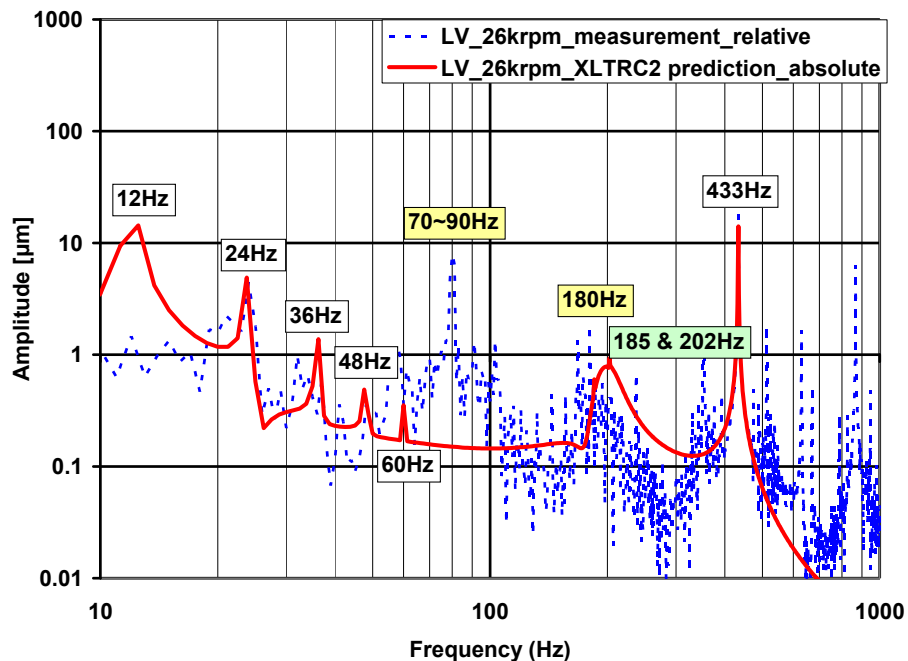


**Fig. D.4 Predicted and measured rotor motion amplitude in frequency domain. Left rotor end vertical direction (LV). Input base excitation frequencies for prediction: 12, 24, 36, 48, 60, 185, and 202 Hz. Rotor speed: 26 krpm (433 Hz).**

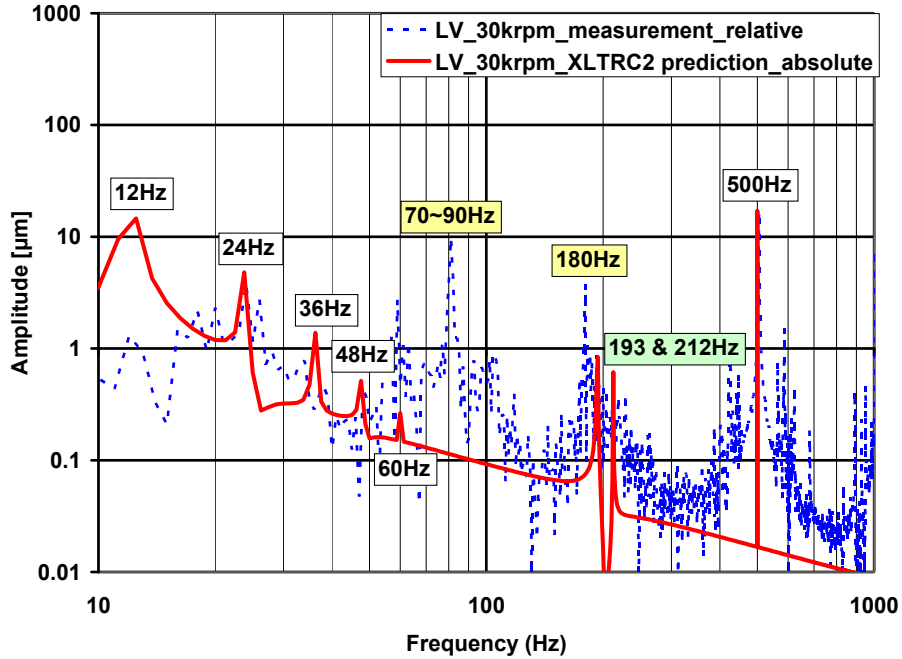


Fig. D.5 Predicted and measured rotor motion amplitude in frequency domain. Left rotor end vertical direction (LV). Input base excitation frequencies for prediction: 12, 24, 36, 48, 60, 193, and 212 Hz. Rotor speed: 30 krpm (500 Hz).

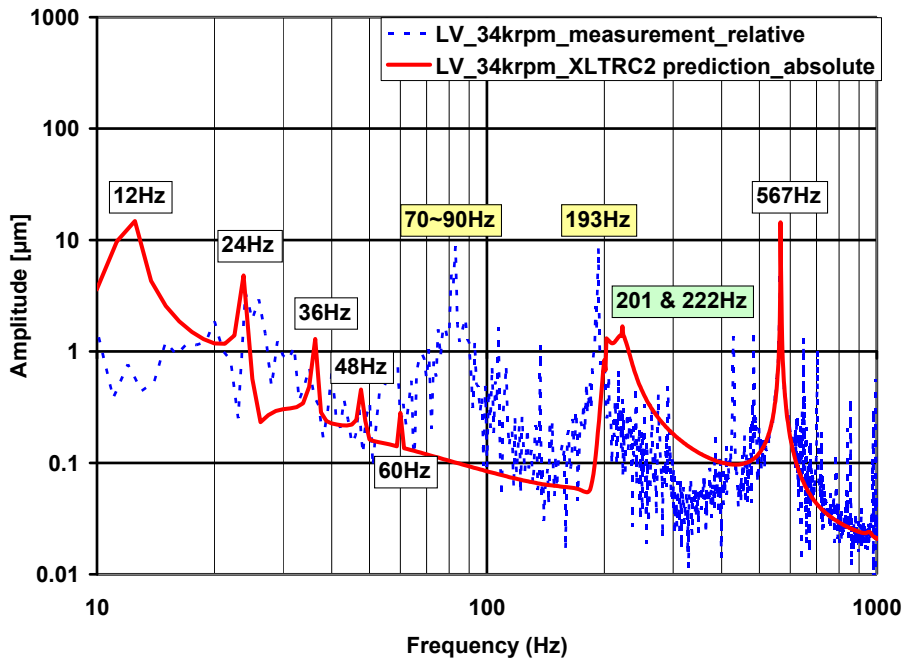


Fig. D.6 Predicted and measured rotor motion amplitude in frequency domain. Left rotor end vertical direction (LV). Input base excitation frequencies for prediction: 12, 24, 36, 48, 60, 201, and 222 Hz. Rotor speed: 34 krpm (567 Hz).

## Appendix E. Rigid rotor model for prediction of rotor motion response due to base excitation

Presently, the rotor is regarded as rigid. Hence, a simple predictive model, rather than using XLTRC<sup>2</sup>®, can be easily programmed using computational software.

The prediction of rotor motion response due to shaker delivered base load excitation is derived from the solution of the following equations of motion:

$$\mathbf{M}\ddot{\mathbf{U}} + \Omega\mathbf{G}\dot{\mathbf{U}} + \mathbf{C}\dot{\mathbf{U}} + \mathbf{K}\mathbf{U} = \mathbf{W} + \mathbf{F}_{\text{imb}} + \mathbf{C}\dot{\mathbf{U}}_{\text{b}} + \mathbf{K}\mathbf{U}_{\text{b}} \quad (\text{E.1})$$

where  $\mathbf{U} = [x_1 \ x_2 \ y_1 \ y_2]^T$  and  $\mathbf{U}_{\text{b}} = [X \ X \ Y \ Y]^T$ , as the vectors of rotor response and base excitation displacements, respectively. The subscripts  $1$  and  $2$  respectively represent the left and right bearing center locations. The coordinate  $x$  denotes horizontal direction, while  $y$  denotes vertical direction. Note that the rotor response and base motions are in an absolute coordinate system. In addition, only vertical base motion is considered, since the base excitation along horizontal direction has insignificant magnitudes. Above  $\Omega$  is the rotor angular speed.  $\mathbf{W} = (0, W, 0, 0)^T$ , with  $W=8.09$  N as the rotor weight.

$\mathbf{M}$ ,  $\mathbf{G}$ ,  $\mathbf{C}$ , and  $\mathbf{K}$  are  $4 \times 4$  inertia, gyroscopic, viscous damping and stiffness matrices, respectively, as originally derived in Ref. [28]:

$$\mathbf{M} = \begin{bmatrix} m \frac{l_1}{l} & m \frac{l_2}{l} & 0 & 0 \\ 0 & 0 & m \frac{l_1}{l} & m \frac{l_2}{l} \\ \frac{I_T}{l} & -\frac{I_T}{l} & 0 & 0 \\ 0 & 0 & -\frac{I_T}{l} & \frac{I_T}{l} \end{bmatrix}; \quad \mathbf{G} = \begin{bmatrix} 0 & 0 & 0 & 0 \\ 0 & 0 & 0 & 0 \\ 0 & 0 & -\frac{I_p}{l} & \frac{I_p}{l} \\ -\frac{I_p}{l} & \frac{I_p}{l} & 0 & 0 \end{bmatrix}; \quad (\text{E.2})$$

$$\mathbf{K} = \begin{bmatrix} K_{xx1} & K_{xx2} & K_{xy1} & K_{xy2} \\ K_{yx1} & K_{yx2} & K_{yy1} & K_{yy2} \\ l_1 K_{xx1} & -l_2 K_{xx2} & l_1 K_{xy1} & -l_2 K_{xy2} \\ -l_1 K_{yx1} & l_2 K_{yx2} & -l_1 K_{yy1} & l_2 K_{yy2} \end{bmatrix}; \quad \mathbf{C} = \begin{bmatrix} C_{xx1} & C_{xx2} & C_{xy1} & C_{xy2} \\ C_{yx1} & C_{yx2} & C_{yy1} & C_{yy2} \\ l_1 C_{xx1} & -l_2 C_{xx2} & l_1 C_{xy1} & -l_2 C_{xy2} \\ -l_1 C_{yx1} & l_2 C_{yx2} & -l_1 C_{yy1} & l_2 C_{yy2} \end{bmatrix}$$

where  $m$  is the rotor mass;  $I_T$  and  $I_p$  are rotor transverse and polar moments of inertia, respectively. Appendix C lists the (synchronous speed) gas bearing stiffness and damping coefficients.  $\mathbf{F}_{\text{imb}}$  is the imbalance force vector in the form of:

$$\mathbf{F}_{\text{imb}} = \begin{bmatrix} m_1 r_1 e^{-j\phi_1} + m_2 r_2 e^{-j\phi_2} \\ jm_1 r_1 e^{-j\phi_1} + jm_2 r_2 e^{-j\phi_2} \\ m_1 r_1 d_1 e^{-j\phi_1} - m_2 r_2 d_2 e^{-j\phi_2} \\ -jm_1 r_1 d_1 e^{-j\phi_1} + jm_2 r_2 d_2 e^{-j\phi_2} \end{bmatrix} \Omega^2 e^{j\Omega t} \quad (\text{E.3})$$

where  $m_1$  and  $m_2$  are the remnant imbalance masses attached at radii  $r_1$  and  $r_2$  at angular locations  $\phi_1$  and  $\phi_2$  on rotor end planes. The imbalance masses and locations are identical with those in XLTRC<sup>2</sup>® predictions.  $d_1$  and  $d_2$  are the distances from the rotor left and right end planes to the rotor center of gravity (CG), respectively.

Equation (E.1) is written in first order form as:

$$\begin{bmatrix} \dot{\mathbf{U}} \\ \ddot{\mathbf{U}} \end{bmatrix} = \begin{bmatrix} \mathbf{0} & \mathbf{I} \\ -\mathbf{M}^{-1}\mathbf{K} & -\mathbf{M}^{-1}(\mathbf{C} + \Omega\mathbf{G}) \end{bmatrix} \begin{bmatrix} \mathbf{U} \\ \dot{\mathbf{U}} \end{bmatrix} + \begin{bmatrix} \mathbf{0} \\ \mathbf{M}^{-1}\mathbf{F} \end{bmatrix} = [\mathbf{A}] \begin{bmatrix} \mathbf{U} \\ \dot{\mathbf{U}} \end{bmatrix} + [\mathbf{b}] \quad (\text{E.4})$$

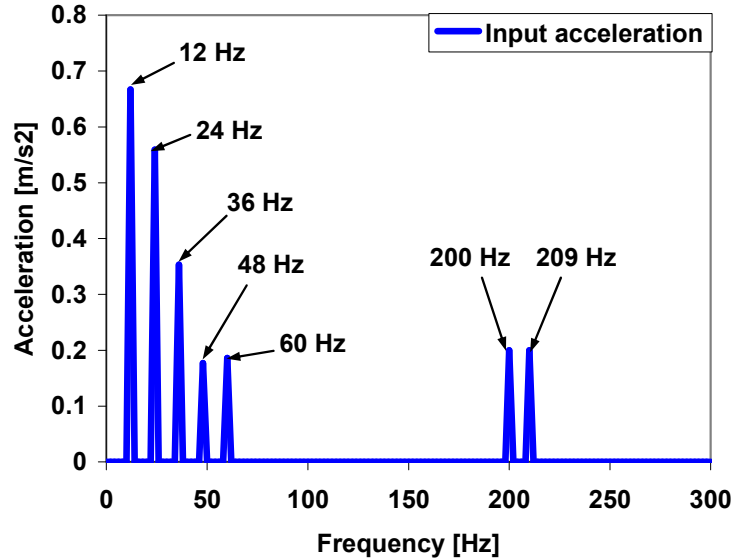
where  $\mathbf{F} = \mathbf{W} + \mathbf{F}_{\text{imb}} + \mathbf{C}\dot{\mathbf{U}}_b + \mathbf{K}\mathbf{U}_b$ , and  $\mathbf{I}$  is the identity matrix.  $\mathbf{A}$  is the parameter matrix, and  $\mathbf{b}$  corresponds to an excitation force vector. The system damped natural frequency is derived from the eigenvalues of  $\mathbf{A}$ , while the eigenvectors represent corresponding mode shapes.

Table E.1 lists the predicted (rigid rotor) natural frequency and mode shapes at three rotor speeds for operation with gas bearing feed pressure equal to 2.36 bar (ab). The predictions from XLTRC<sup>2</sup>®, Table D.1, and the measured values are included for comparison. The cylindrical mode natural frequency predicted by both models is nearly identical. However, the conical mode natural frequency derived from the rigid rotor model is ~13 Hz lower. Rotor flexibility may not explain the (relatively minor) differences.

**Table E.1 Estimated damped natural frequency and mode shapes from rigid rotor model. Gas bearing supply pressure=2.36 bar (ab).**

Rotor speed	26 krpm	30 krpm	34 krpm
<b>Conical</b>	191 Hz	200 Hz	208 Hz
<b>Cylindrical</b>	184 Hz	192 Hz	200 Hz
<b>XLTRC<sup>2</sup></b>			
<b>Conical</b>	202 Hz	212 Hz	222 Hz
<b>Cylindrical</b>	185 Hz	193 Hz	201 Hz
<b>Measured</b>			
<b>Cylindrical</b>	180 Hz	180 Hz	193 Hz

Figure E.1 shows the input acceleration when the rotor operates at 34 krpm. See Figure 9(d) for the measured base acceleration. Note that 200 and 209 Hz are the (predicted) rotor-bearing system natural frequencies at 34 krpm.



**Fig. E.1 Input base excitation acceleration for prediction of rotor response. Rotor speed: 34 krpm. Main excitation frequency 12 Hz.**

Note that only the steady-state periodic rotor motion response is of interest. The excitation loads include base motion induced forces and remnant imbalance forces. The system response equals to the superposition of unique single frequency responses, each obtained separately from Eq. (E.4). Since the calculated rotor response refers to an absolute coordinate system, the base motion is subtracted from the calculated rotor response. In this form, rotor motion amplitudes relative to the (moving) bearing housing are obtained.

For example, for a forcing function of the form  $\mathbf{F} e^{i\omega t}$ , the rotor periodic response is at the same frequency  $\omega$ , i.e.  $\mathbf{Z} e^{i\omega t}$ . Hence, the analytical solution of Eq. (E.1) gives the complex amplitude response

$$\mathbf{Z} = \left[ \mathbf{K} - \omega^2 \mathbf{M} + i\Omega \omega \mathbf{G} + i\omega \mathbf{C} \right]^{-1} \mathbf{F} \quad (\text{E.5})$$

For rotor speeds equal to 26, 30 and 34 krpm, Figures E.2, E.3 and E.4 depict the predicted and measured displacements at the rotor left end, vertical direction (LV). The graphs include predictions for both the absolute and relative (to base) rotor displacements.

Absolute and relative rotor amplitude motions are nearly identical for excitation frequencies well above the system natural frequencies, i.e. the rotor synchronous motion, for example. When the rotor spins at (say) 30 krpm (500 Hz), the rotor-bearing system operates in an inertial mode since this frequency is well above the natural frequency of the rotor-bearing system.

The measured and predicted motion components with synchronous frequency are in agreement. The predicted displacement amplitudes at the natural frequency are lesser than the measured ones, in particular at rotor speed of 34 krpm. That is, the actual test system has lesser damping than that used in the predictions.

Since the base excitation is of low frequency (12 Hz) and its harmonics, the differences between absolute and relative displacements are apparent. The predicted amplitudes of rotor motion relative to the base, at 12 Hz and its harmonics, are of similar amplitude as the measured ones, except the responses at 24 Hz. As with the measured displacement amplitude component at the natural frequency, the predicted amplitude of increases in magnitude as the rotor speed increases, indicating lesser damping.

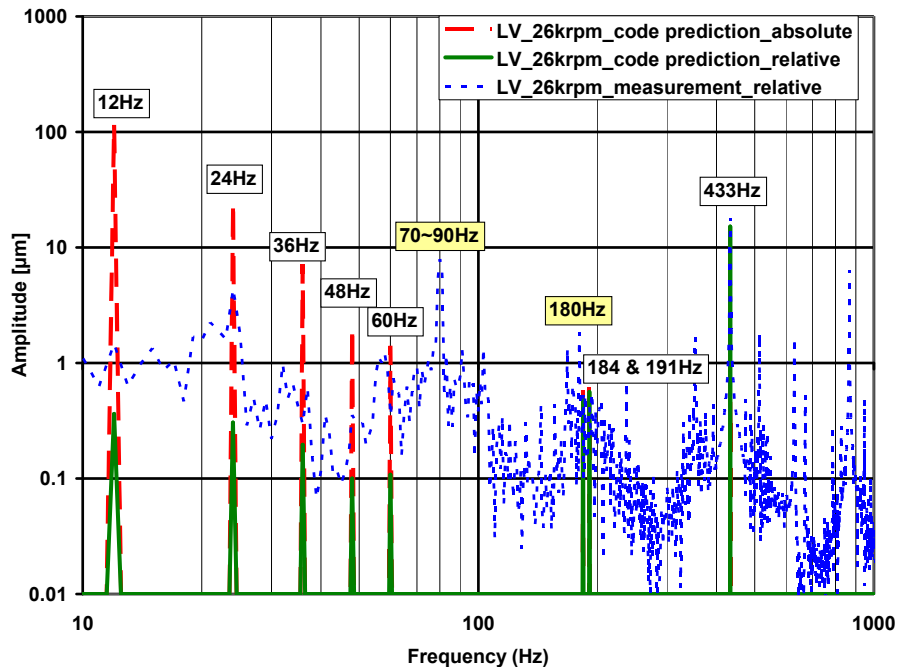


**Fig. E.2 Predicted and measured rotor response amplitude. Left rotor end vertical direction (LV). Input base excitation frequencies for prediction: 12, 24, 36, 48, 60, 184, and 191 Hz. Rotor speed: 26 krpm (433 Hz).**



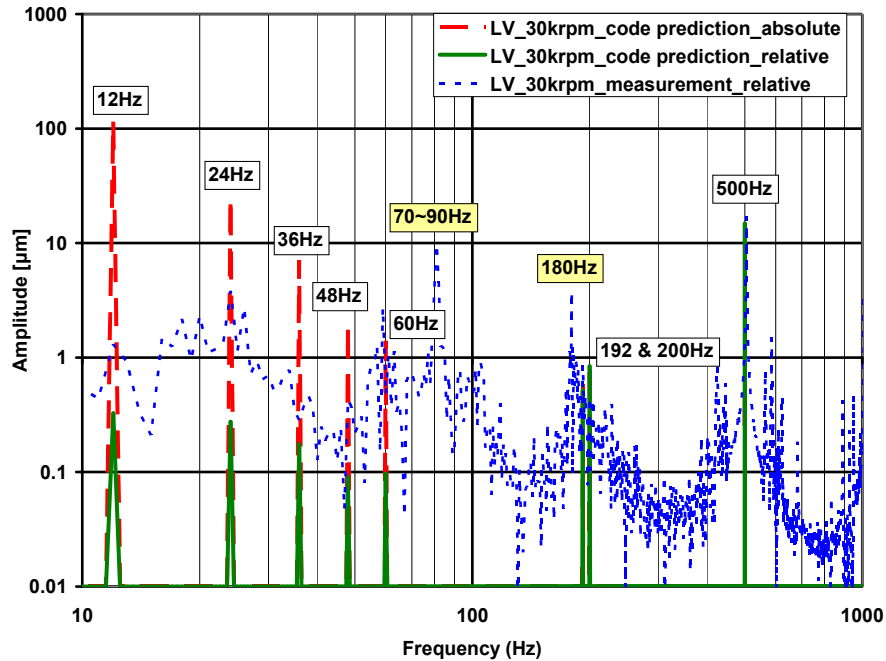


Fig. E.3 Predicted and measured rotor response amplitude. Left rotor end vertical direction (LV). Input base excitation frequencies for prediction: 12, 24, 36, 48, 60, 192, and 200 Hz. Rotor speed: 30 krpm (500 Hz).

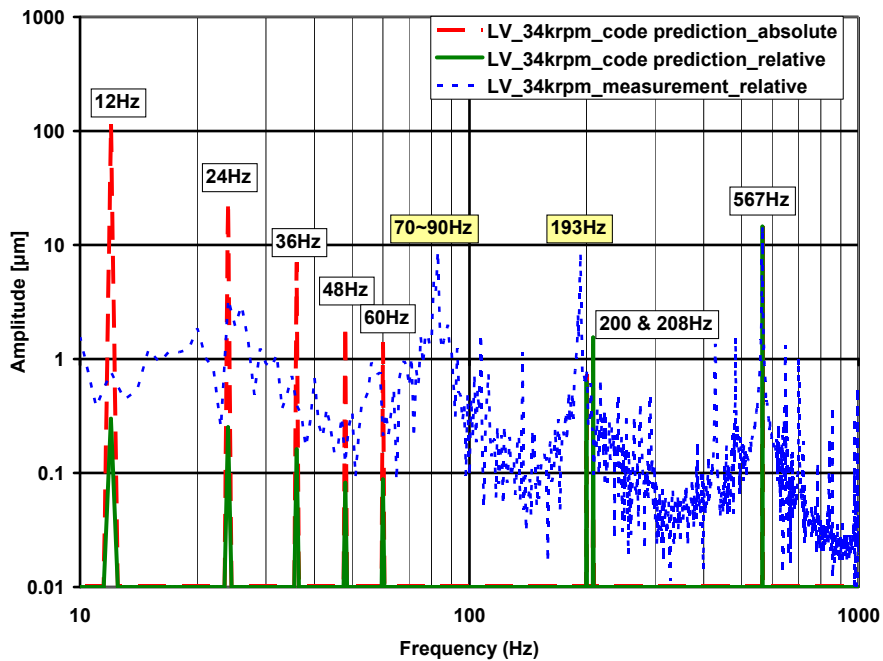


Fig. E.4 Predicted and measured rotor response amplitude. Left rotor end vertical direction (LV). Input base excitation frequencies for prediction: 12, 24, 36, 48, 60, 200, and 208 Hz. Rotor speed: 34 krpm (567 Hz).

Figure E.5 compares the absolute motion amplitudes predicted by XLTRC<sup>2</sup>® and the rigid rotor model while the rotor spins at 30 krpm. The motion amplitude component at the frequency synchronous with running speed is the same for both models since the imbalance distribution is the same. Both amplitude components at the natural frequency are similar in magnitude, albeit the natural frequencies from the two predictive models are slightly different (~13 Hz difference). For the base motion, at 12 Hz and its harmonics, XLTRC<sup>2</sup>® predicts absolute motions that are lower than those predicted (exactly) by the rigid rotor model. The differences are ascribed to the sampling rate (time step) used in the numerical integration of the equations of motion.

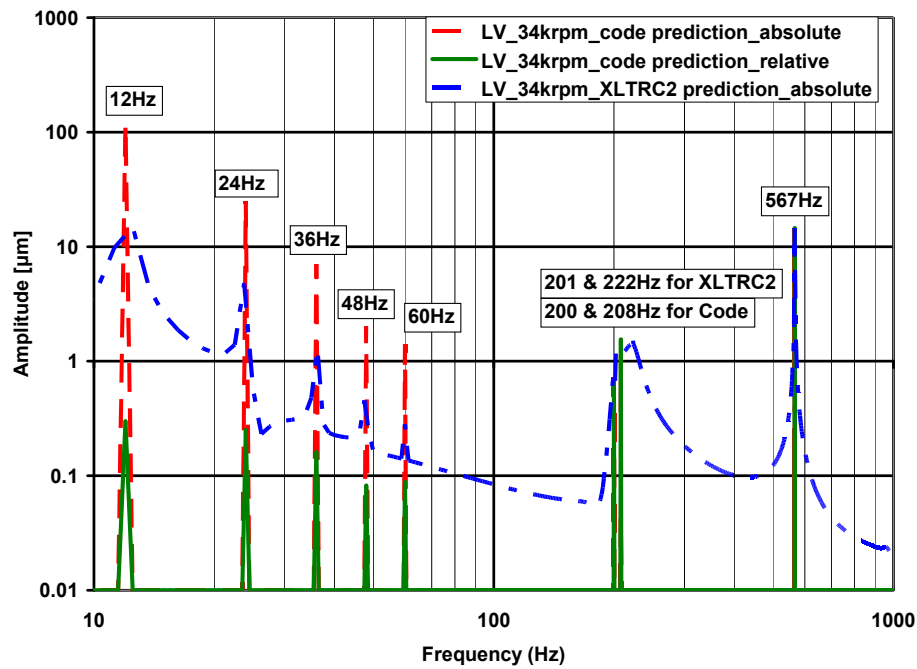


Fig. E.5 Comparison of predicted absolute rotor displacements from rigid rotor model and XLTRC<sup>2</sup>®. Left rotor end vertical direction (LV). Rotor speed: 34 krpm (567 Hz).